Contents lists available at ScienceDirect

Planetary and Space Science

Scientific rationale for Saturn's *in situ* exploration

O. Mousis [a,*], L.N. Fletcher [b], J.-P. Lebreton [c,d], P. Wurz [e], T. Cavalié [f], A. Coustenis [d], R. Courtin [d], D. Gautier [d], R. Helled [g], P.G.J. Irwin [b], A.D. Morse [h], N. Nettelmann [i], B. Marty [j], P. Rousselot [a], O. Venot [k], D.H. Atkinson [l,n], J.H. Waite [m], K.R. Reh [n], A.A. Simon [o], S. Atreya [p], N. André [q], M. Blanc [q], I.A. Daglis [r], G. Fischer [s], W.D. Geppert [t], T. Guillot [u], M.M. Hedman [v], R. Hueso [w,x], E. Lellouch [d], J.I. Lunine [y], C.D. Murray [z], J. O'Donoghue [aa], M. Rengel [f], A. Sánchez-Lavega [w,x], F.-X. Schmider [u], A. Spiga [ab], T. Spilker [ac], J.-M. Petit [a], M.S. Tiscareno [y], M. Ali-Dib [a], K. Altwegg [e], S.J. Bolton [m], A. Bouquet [a,m], C. Briois [c], T. Fouchet [d], S. Guerlet [ab], T. Kostiuk [o], D. Lebleu [ad], R. Moreno [d], G.S. Orton [n], J. Poncy [ad]

[a] Université de Franche-Comté, Institut UTINAM, CNRS/INSU, UMR 6213, Observatoire des Sciences de l'Univers de Besançon, France
[b] Atmospheric, Oceanic & Planetary Physics, Department of Physics, University of Oxford, Clarendon Laboratory, Parks Road, Oxford OX1 3PU, UK
[c] LPC2E, CNRS-Université d'Orléans, 3a Avenue de la Recherche Scientifique, 45071 Orléans Cedex 2, France
[d] LESIA, Observatoire de Paris, CNRS, UPMC, Univ. Paris-Diderot, 5, place Jules Janssen, F-92195 Meudon Cedex, France
[e] Space Science & Planetology, Physics Institute, University of Bern, Sidlerstrasse 5, 3012 Bern, Switzerland
[f] Max-Planck-Institut für Sonnensystemforschung, Justus-von-Liebig-Weg 3, 37077 Göttingen, Germany
[g] Department of Geophysics, Atmospheric and Planetary Sciences, Tel-Aviv University, Tel-Aviv, Israel
[h] Planetary and Space Sciences, Department of Physics, The Open University, Walton Hall, Milton Keynes MK7 6AA, UK
[i] Institute for Physics, University of Rostock, 18051 Rostock, Germany
[j] CRPG-CNRS, Nancy-Université, 15 rue Notre Dame des Pauvres, 54501 Vandoeuvre-ls-Nancy, France
[k] Instituut voor Sterrenkunde, Katholieke Universiteit Leuven, Celestijnenlaan 200D, 3001 Leuven, Belgium
[l] Department of Electrical and Computer Engineering, University of Idaho, Moscow, ID 83844-1023, USA
[m] Southwest Research Institute (SwRI), 6220 Culebra Road, San Antonio, TX 78228, USA
[n] Jet Propulsion Laboratory, California Institute of Technology, 4800 Oak Grove Drive, Pasadena, CA 91109, USA
[o] NASA Goddard Space Flight Center, Code 690, Greenbelt, MD 20771, USA
[p] Department of Atmospheric, Oceanic, and Space Sciences, University of Michigan, Ann Arbor, MI 48109-2143, USA
[q] Institut de Recherche en Astrophysique et Planétologie (IRAP), CNRS/Université Toulouse III (UMR 5277), 9, avenue du Colonel Roche, BP 44346, 31028 Toulouse Cedex 4, France
[r] University of Athens, Department of Physics, Panepistimioupoli Zografou, 15784 Athens, Greece
[s] Space Research Institute, Austrian Academy of Sciences, Schmiedlstrasse 6, A-8042 Graz, Austria
[t] Stockholm University Astrobiology Centre, Department of Physics, AlbaNova, Stockholm University/Stockholms universitet, Roslagstullsbacken 21, S-10691 Stockholm, Sweden/Sverige
[u] Observatoire de la Côte d'Azur, Laboratoire Lagrange, BP 4229, 06304 Nice cedex 4, France
[v] Department of Physics, University of Idaho, Moscow ID 83843
[w] Departamento Física Aplicada I, Universidad del País Vasco UPV/EHU, ETS Ingeniería, Alameda Urquijo s/n, 48013 Bilbao, Spain
[x] Unidad Asociada Grupo Ciencias Planetarias UPV/EHU-IAA(CSIC), 48013 Bilbao, Spain
[y] Center for Radiophysics and Space Research, Space Sciences Building, Cornell University, Ithaca, NY 14853, USA
[z] School of Physics and Astronomy, Queen Mary University of London, Mile End Road, London E1 4NS, UK
[aa] Department of Physics and Astronomy, University of Leicester, Leicester LE1 7RH, UK
[ab] Laboratoire de Météorologie Dynamique, Université Pierre et Marie Curie, Institut Pierre Simon Laplace, Paris, France
[ac] Solar System Science & Exploration, Monrovia, USA
[ad] Thales Alenia Space, Cannes, France

ARTICLE INFO

ABSTRACT

Remote sensing observations meet some limitations when used to study the bulk atmospheric composition of the giant planets of our solar system. A remarkable example of the superiority of *in situ* probe measurements is illustrated by the exploration of Jupiter, where key measurements such as the determination of the noble gases' abundances and the precise measurement of the helium mixing ratio have only been made available through *in situ* measurements by the Galileo probe. This paper describes the main scientific goals to be addressed by the future *in situ* exploration of Saturn placing the

* Corresponding author.
E-mail address: olivier.mousis@obs-besancon.fr (O. Mousis).

Galileo probe exploration of Jupiter in a broader context and before the future probe exploration of the more remote ice giants. *In situ* exploration of Saturn's atmosphere addresses two broad themes that are discussed throughout this paper: first, the formation history of our solar system and second, the processes at play in planetary atmospheres. In this context, we detail the reasons why measurements of Saturn's bulk elemental and isotopic composition would place important constraints on the volatile reservoirs in the protosolar nebula. We also show that the *in situ* measurement of CO (or any other disequilibrium species that is depleted by reaction with water) in Saturn's upper troposphere may help constraining its bulk O/H ratio. We compare predictions of Jupiter and Saturn's bulk compositions from different formation scenarios, and highlight the key measurements required to distinguish competing theories to shed light on giant planet formation as a common process in planetary systems with potential applications to most extrasolar systems. *In situ* measurements of Saturn's stratospheric and tropospheric dynamics, chemistry and cloud-forming processes will provide access to phenomena unreachable to remote sensing studies. Different mission architectures are envisaged, which would benefit from strong international collaborations, all based on an entry probe that would descend through Saturn's stratosphere and troposphere under parachute down to a minimum of 10 bar of atmospheric pressure. We finally discuss the science payload required on a Saturn probe to match the measurement requirements.

1. Introduction

Giant planets contain most of the mass and the angular momentum of our planetary system and must have played a significant role in shaping its large scale architecture and evolution, including that of the smaller, inner worlds (Gomes et al., 2005). Furthermore, the formation of the giant planets affected the timing and efficiency of volatile delivery to the Earth and other terrestrial planets (Chambers and Wetherill, 2001). Therefore, understanding giant planet formation is essential for understanding the origin and evolution of the Earth and other potentially habitable environments throughout our solar system. The origin of the giant planets, their influence on planetary system architectures, and the plethora of physical and chemical processes at work within their atmospheres make them crucial destinations for future exploration. Because Jupiter and Saturn have massive envelopes essentially composed of hydrogen and helium and (possibly) a relatively small core, they are called gas giants. Meanwhile, Uranus and Neptune also contain hydrogen and helium atmospheres but, unlike Jupiter and Saturn, their H_2 and He mass fractions are smaller (5–20%). They are called ice giants because their density is consistent with the presence of a significant fraction of ices/rocks in their interiors. Despite this apparent grouping into two classes of giant planets, the four giant planets likely exist on a continuum, each a product of the particular characteristics of their formation environment. Comparative planetology of the four giants in the solar system is therefore essential to reveal the potential formational, migrational, and evolutionary processes at work during the early evolution of the early solar nebula.

Much of our understanding of the origin and evolution of the outer planets comes from remote sensing by necessity. However, the efficiency of this technique has limitations when used to study the bulk atmospheric composition that is crucial to the understanding of planetary origin, namely due to degeneracies between the effects of temperatures, clouds and abundances on the emergent spectra, but also due to the limited vertical resolution. In addition, many of the most common elements are locked away in a condensed phase in the upper troposphere, hiding the main volatile reservoir from the reaches of remote sensing. It is only by penetrating below the "visible" weather layer that we can sample the deeper troposphere where those most common elements are well mixed. A remarkable example of the superiority of *in situ* probe measurements is illustrated by the exploration of Jupiter, where key measurements such as the determination of the noble gases' abundances and the precise measurement of the helium mixing ratio have only been possible through *in situ* measurements by the Galileo probe (Owen et al., 1999).

The Galileo probe measurements provided new insights into the formation of the solar system. For instance, they revealed the

unexpected enrichments of Ar, Kr and Xe with respect to their solar abundances, which suggested that the planet accreted icy planetesimals formed at temperatures possibly as low as 20–30 K to allow the trapping of these noble gases. Another remarkable result was the determination of the Jovian helium abundance using a dedicated instrument aboard the Galileo probe (von Zahn et al., 1998) with an accuracy of 2%. Such an accuracy on the He/H_2 ratio is impossible to derive from remote sensing, irrespective of the giant planet being considered, and yet precise knowledge of this ratio is crucial for the modelling of giant planet interiors and thermal evolution. The Voyager mission has already shown that these ratios are far from being identical, which presumably results from slight differences in their histories at different heliocentric distances. An important result also obtained by the mass spectrometer onboard the Galileo probe was the determination of the $^{14}N/^{15}N$ ratio, which suggested that nitrogen present in Jupiter today originated from the solar nebula essentially in the form of N_2 (Owen et al., 2001). The Galileo science payload unfortunately could not probe to pressure levels deeper than 22 bar, precluding the determination of the H_2O abundance at levels representative of the bulk oxygen enrichment of the planet. Furthermore, the probe descended into a region depleted in volatiles and gases by unusual "hot spot" meteorology (Orton et al., 1998; Wong et al., 2004), and therefore its measurements are unlikely to represent the bulk planetary composition. Nevertheless, the Galileo probe measurements were a giant step forward in our understanding of Jupiter. However, with only a single example of a giant planet measurement, one must wonder whether from the measured pattern of elemental and isotopic enrichments, the chemical inventory and formation processes at work in our solar system are truly understood. *In situ* exploration of giant planets is the only way to firmly characterize the planet compositions in the solar system. In this context, a Saturn probe is the next natural step beyond Galileo's *in situ* exploration of Jupiter, the remote investigation of its interior and gravity field by the JUNO mission, and the Cassini spacecraft's orbital reconnaissance of Saturn.

In situ exploration of Saturn's atmosphere addresses two broad themes. First, the formation history of our solar system and second, the processes at play in planetary atmospheres. Both of these themes are discussed throughout this paper. Both themes have relevance far beyond the leap in understanding gained about an individual giant planet: the stochastic and positional variances produced within the solar nebula, the depth of the zonal winds, the propagation of atmospheric waves, the formation of clouds and hazes and disequilibrium processes of photochemistry and vertical mixing are common to all planetary atmospheres, from terrestrial planets to gas and ice giants and from brown dwarfs to hot exoplanets.

This paper describes the main scientific goals to be addressed by the future *in situ* exploration of Saturn placing the Galileo probe exploration of Jupiter in a broader context and before the future *in situ* exploration of the more remote ice giants. These goals will become the primary objectives listed in the forthcoming Saturn probe proposals that we intent to submit in response to future opportunities within both ESA and NASA. Section 2 is devoted to a comparison between known elemental and isotopic compositions of Saturn and Jupiter. We describe the different formation scenarios that have been proposed to explain Jupiter's composition and discuss the key measurements at Saturn that would allow disentangling these interpretations. We also demonstrate that the *in situ* measurement of CO (or any other disequilibrium species that is depleted by reaction with water) at Saturn could place limits on its bulk O/H ratio. In Section 3, we discuss the motivation for the *in situ* observation of the atmospheric processes (dynamics, chemistry and cloud formation) at work in Saturn's atmosphere. Section 4 is dedicated to a short description of the mission designs that can be envisaged. In Section 5, we provide a description of high-level specifications for the science payload. Conclusions are given in Section 6.

2. Elemental and isotopic composition as a window on Saturn's formation

The giant planets in the solar system formed 4.55 Gyr ago from the same material that engendered the Sun and the entire solar system. The envelopes of giant planets are dominated by hydrogen and helium, the two most abundant elements in the Universe. Protoplanetary disks, composed of gas and dust, are almost ubiquitous when stars form, but their typical lifetimes do not exceed a few million years. This implies that the gas giants Jupiter and Saturn had to form rapidly to capture their hydrogen and helium envelopes, more rapidly than the tens of millions of years needed for terrestrial planets to reach their present masses (Pollack et al., 1996; Alibert et al., 2005a,b). Due to formation at fairly large radial distances from the Sun, where the solid surface density is low, the ice giants Uranus and Neptune had longer formation timescales (slow growth rates) and did not manage to capture large amounts of hydrogen and helium before the disk gas dissipated (Dodson-Robinson and Bodenheimer, 2010; Helled and Bodenheimer, 2014). As a result, the masses of their gaseous envelopes are small compared to their ice/rock cores.

A comparative study of the properties of these giant planets thus gives information on spatial gradients in the physical/chemical properties of the solar nebula as well as on stochastic effects[1] that led to the formation of the solar system. Data on the composition and structure of the giant planets, which hold more than 95% of the non-solar mass of the solar system, remain scarce, despite the importance of such knowledge. The formation of giant planets is now largely thought to have taken place via the core accretion model in which a dense core is first formed by accretion and the hydrogen–helium envelope is captured after a critical mass is reached (Mizuno, 1980; Pollack et al., 1996). When the possibility of planet migration is included (Lin and Papaloizou, 1986; Ward, 1997), such a model can explain the orbital properties

of exoplanets, although lots of unresolved issues remain (Ida and Lin, 2004; Mordasini et al., 2012). However, an alternative scenario for the formation of giant planets is the disk instability model (Boss, 1997, 2001), in which the giant planets form from the direct contraction of a gas clump resulting from local gravitational instability in the disk.

Formation and evolution models indicate that the total mass of heavy elements present in Jupiter may be as high as 42 $M_\oplus$, whereas the mass of the core is estimated to range between 0 and 13 $M_\oplus$ (Saumon and Guillot, 2004). In the case of Saturn, the mass of heavy elements can be as large as 35 $M_\oplus$ with a mass varying between 0 and 10 $M_\oplus$ in the envelope and the core mass ranging between 0 and 20 $M_\oplus$ (Helled and Guillot, 2013). Direct access to heavy materials within giant planet cores to constrain these models is impossible, so we must use the composition of the well-mixed troposphere to infer the properties of the deep interiors. It is difficult for remote sounding to provide the necessary information because of a lack of sensitivity to the atmospheric compositions beneath the cloudy, turbulent and chaotic weather layer. These questions must be addressed by *in situ* exploration, even if the NASA JUNO mission will try to address them remotely.

The availability of planetary building blocks (metals, oxides, silicates, ices) is expected to vary with position within the original nebula, from refractories in the warm inner nebula to a variety of ices of water, CH_4, CO, NH_3, N_2 and other simple molecules in the cold outer nebula. Turbulent radial mixing, and the evolution of the pressure–temperature gradient in the disk could have led to distinct regions where some species dominated over others (*e.g.*, the water ice snowline or N_2 over NH_3). Furthermore, both inward and outward migration of the giants during their evolution could have provided access to different material reservoirs at different epochs. A giant planet's bulk composition therefore depends on the timing and location of planet formation, subsequent migration and the delivery mechanisms for the heavier elements. By measuring a giant planet's chemical inventory, and contrasting it with measurements of (i) other giant planets, (ii) primitive materials found in comets and asteroids, and (iii) the elemental abundances of our parent star and the local interstellar medium, we can reveal much about the conditions at work during the formation of our planetary system. Furthermore, measurements of atmospheric bulk elemental enrichments and isotopic ratios would help us to distinguish between the existing formation scenarios (see Section 2.4 for details).

It should be noted, however, that when atmospheric measurements are used to infer the planetary composition and reveal information on the planet's origin, one has to *assume* that the atmospheric composition is illustrative of the composition of the building blocks accreted by the envelope. This is a fairly good assumption in the case of a gas giant if the measurement probes a convective region, and if the planet is fully convective. Within a fully convective planet the materials are expected to be homogeneously mixed, and therefore, we do not expect large differences in composition with depth. However, if the planet is not fully convective and homogeneously mixed, the information of its atmospheric composition cannot solely be used to infer the bulk composition.

In the case of Saturn (as well as Jupiter) compositional inhomogeneities can be the outcome of the formation process (*e.g.*, Pollack et al., 1996) and/or the erosion of a primordial core that could mix with the surrounding metallic hydrogen (Guillot, 2004; Wilson and Militzer, 2011, 2012). In addition, it is possible that double diffusive convection occurs in the interiors of giant planets (*e.g.*, Leconte and Chabrier, 2012, 2013). If a molecular weight gradient is maintained throughout the planetary envelope, double-diffusive convection would take place, and the thermal structure would be very different from the one that is generally assumed using adiabatic (*i.e.*, fully convective)

---

[1] Although the equations of evolution of the early Solar System are deterministic, they are sensitive to the exact initial conditions. This results in a stochastic-like evolution. Consider for example the collision that induced the large obliquity of Uranus or the one that created the Moon from proto-Earth. In both cases, a large planetesimal or planetary embryo (Earth-mass for Uranus and Mars-mass for the Earth) happened to cross the orbit of the planet and hit it at exactly the right location to get the desired effect. A very slight variation of the impact location would have had a very different output, with a low obliquity for Uranus, or no Moon around the Earth (and thus no evolution of intelligent life on Earth).

models, with much higher center temperatures and a larger fraction of heavy elements. In this case, the planetary composition can vary substantially with depth and therefore, a measured composition of the envelope would not represent the overall composition. While standard interior models of Saturn assumed three layers and similar constraints in terms of the helium to hydrogen ratio, they can differ in the assumption on the distribution of heavy elements within the planetary envelope. While Guillot and collaborators (*e.g.*, Saumon and Guillot, 2004; Helled and Guillot, 2013) assume homogeneous distribution of heavy elements apart from helium, which is depleted in the outer envelope due to helium rain,[2] interior structure models by Nettelmann and collaborators (Fortney and Nettelmann, 2010; Nettelmann et al., 2013) allow the abundance of heavy elements to be discontinuous between the molecular and the metallic envelope. At present, it is not clear whether there should be a discontinuity in the composition of heavy elements, and this question remains open.

2.1. Jupiter and Saturn's composition

The abundances and isotopic ratios of most significant volatiles measured at Jupiter and Saturn are given in Tables 1 and 2. We refer the reader to the papers of Atreya et al. (2003), Teanby et al. (2006) and Fletcher et al. (2012) for a more exhaustive list of disequilibrium species identified (or for other minor species presumably identified) in Jupiter's and Saturn's atmospheres. Only upper limits on the abundances of hydrogen halides have been derived from the remote detection of these species in Saturn's atmosphere, implying the need of a probe to get improved *in situ* measurements.

The abundances of CH_4, NH_3, H_2O, H_2S, Ne, Ar, Kr and Xe have been measured by the Galileo Probe Mass Spectrometer (GPMS) in Jupiter's atmosphere (Mahaffy et al., 2000; Wong et al., 2004). The value of H_2O abundance reported for Jupiter in Table 1 corresponds to the deepest measurement made by the probe (at 17.6–20.9 bar) and is probably much smaller than the planet's bulk water abundance, which remains unknown (Atreya et al., 2003; Wong et al., 2004). The Juno mission, which will arrive at Jupiter in 2016, may provide an estimate of the tropospheric O/H ratio. The He abundance in Jupiter has also been measured *in situ* by a Jamin–Mascart interferometer aboard the Galileo probe (Helium Abundance Detector; hereafter HAD) with a better accuracy level than the GPMS instrument (von Zahn et al., 1998). PH_3 is the only species of our list of Jupiter measurements whose abundance has been determined remotely by the Cassini Composite Infrared Spectrometer (CIRS) during the spacecraft 2000–2001 encounter (Fletcher et al., 2009a). PH_3 is a disequilibrium species at its sampling level in Jupiter's atmosphere (see Section 3). However, because (i) it is the dominating P-bearing species at the quench level (Fegley and Prinn, 1985) and (ii) its destruction rate is inhibited at low temperature, the measured PH_3 value, if correct, must be close to the bulk P abundance. Isotopic measurements presented for Jupiter in Table 2 have also been performed by the GPMS instrument aboard the Galileo probe (Niemann et al., 1996, 1998; Mahaffy et al., 2000; Atreya et al., 2003; Wong et al., 2004).

In the case of Saturn, only the abundances of CH_4, PH_3, NH_3, H_2O, and indirectly that of H_2S, have been measured. The abundance of CH_4 has been determined from the analysis of high spectral resolution observations from CIRS (Fletcher et al., 2009b). Similar to Jupiter, PH_3 has been determined remotely in Saturn from Cassini/CIRS observations at 10 μm (Fletcher et al., 2009a). Other measurements of PH_3 have been made from ground based

observations at 5 μm (de Graauw et al., 1997), but the spectral line data at these wavelengths is less robust and accurate than those at 10 μm. There is also a degeneracy with the location, extent, opacity of Saturn's clouds at 5 μm which is not apparent at 10 μm. Moreover, considering the fact that there is also terrestrial contamination in the 5 μm window for ground-based observations and that the scattered sunlight may contribute at 5 μm, this leads us to believe that the data at 10 μm are more reliable. Interestingly, we note that PH_3 is easier to detect on Saturn compared to Jupiter because this molecule dominates the upper tropospheric chemistry and ammonia is locked away at deeper levels. The NH_3 abundance corresponds to the highest/deepest value derived by Fletcher et al. (2011) who analyzed Saturn's tropospheric composition from Cassini/VIMS 4.6–5.1 μm thermal emission spectroscopy. This determination is probably more reliable than those made in the microwave domain because of the absence of spectral lines at these wavelengths (Briggs and Sackett, 1989; Laraia et al., 2013). Tropospheric H_2O has been inferred in Saturn via the Short Wavelength Spectrometer Instrument onboard the Infrared Space Observatory (ISO-SWS) (de Graauw et al., 1997). However, H_2O is unsaturated at this altitude (∼3 bar level), implying that its bulk abundance is higher than the measured one. The H_2S abundance is quoted from the indirect determination of Briggs and Sackett (1989) who investigated the influence of models of NH_3–H_2S–H_2O cloud decks on Saturn's atmospheric opacity at microwave wavelengths. The He abundance in Saturn's atmosphere derives from a reanalysis of Voyager's infrared spectrometer (IRIS) measurements (Conrath and Gautier, 2000). The only isotopic ratios measured in Saturn are D/H in H_2 (determination from ISOSWS, Lellouch et al., 2001) and $^{12}C/^{13}C$ in CH_4 (Cassini/CIRS observations, Fletcher et al., 2009b).

Table 3 summarizes the enrichments in volatiles relative to protosolar values observed in Jupiter and Saturn. Note that protosolar abundances are different from present-day solar photospheric abundances because elements heavier than He are settling out of the photosphere over time. This mechanism leads to a fractionation of heavy elements relative to hydrogen in the solar photosphere, requiring the use of correction terms to retrieve the protosolar abundances (Lodders et al., 2009). For the sake of information, the protosolar elemental abundances used in our calculations are detailed in Table 4. C, N, P, S, Ar, Kr and Xe are all found enriched by a factor ∼2–4 in Jupiter. On the other hand, C, N and P (the only heavy elements *a priori* reliably measured) are found enriched by factors of ∼10, 0.5–5 and 11.5 in Saturn. Helium is depleted compared to protosolar values in the two giants because of its condensation into droplets that "rain out" in the giant planets deep interiors (Stevenson and Salpeter, 1977a,b; Fortney and Hubbard, 2003). The solution of neon in those droplets (Wilson and Militzer, 2010) would also explain its apparent depletion in Jupiter but a similar measurement has never been possible on Saturn. As mentioned above, oxygen is also depleted compared to protosolar in the Jovian atmosphere but this measurement results from the fact that the Galileo probe entry site was an unusually dry meteorological system. As a result, the probe did not measure the deep, well-mixed water mixing ratio (Wong et al., 2004), which is predicted to be supersolar (Stevenson and Lunine, 1988; Gautier et al., 2001; Hersant et al., 2004; Alibert et al., 2005a; Mousis et al., 2009, 2012).

2.2. Indirect determination of Saturn's O/H ratio

One of the main objectives of Saturn's *in situ* exploration is the measurement of the H_2O abundance. However, depending on the O/H elemental enrichment (Atreya et al., 1999), H_2O is predicted to condense in the 12.6–21 bar range and may remain out of reach for the probe we consider in this paper that would be limited to ∼10 bar (see Section 4). Several disequilibrium species, like CO,

---

[2] A process that is due to helium immiscibility in hydrogen. In this case, helium droplets nucleate from the supersaturated mixture and fall under the influence of gravity, despite the convection in the envelope (Stevenson and Salpeter, 1977a,b).

Table 1
Observed compositions of the atmospheres of Jupiter and Saturn (major volatiles).

Species	Jupiter			Saturn		
	X/H_2	$\Delta(X/H_2)$	Reference	X/H_2	$\Delta(X/H_2)$	Reference
CH_4	2.37×10^{-3}	5.70×10^{-4}	Wong et al. (2004)	5.33×10^{-3}	2.30×10^{-4}	Fletcher et al. (2009b)
NH_3	6.64×10^{-4}	2.54×10^{-4}	Wong et al. (2004)	4.54×10^{-4}	1.14×10^{-4}	Fletcher et al. (2011)
H_2O[a]	4.90×10^{-4}	1.60×10^{-4}	Wong et al. (2004)	2.0×10^{-7}	–	de Graauw et al. (1997)
PH_3	2.15×10^{-6}	1.16×10^{-7}	Fletcher et al. (2009a)	7.28×10^{-6}	4.80×10^{-7}	Fletcher et al. (2009a)
H_2S	8.90×10^{-5}	2.10×10^{-5}	Wong et al. (2004)	3.76×10^{-4}	–	Briggs and Sackett (1989)
He	1.57×10^{-1}	3.00×10^{-3}	von Zahn et al. (1998)	1.35×10^{-1}	2.50×10^{-2}	Conrath and Gautier (2000)
Ne[b]	2.48×10^{-5}	2.80×10^{-7}	Mahaffy et al. (2000)	–	–	
Ar	1.82×10^{-5}	3.60×10^{-6}	Mahaffy et al. (2000)	–	–	
Kr	9.30×10^{-9}	1.70×10^{-9}	Mahaffy et al. (2000)	–	–	
Xe	8.90×10^{-10}	1.70×10^{-10}	Mahaffy et al. (2000)	–	–	

$\Delta(X/H_2)$ represents the uncertainty on measurement.

[a] This is a lower limit.

[b] This is an upper limit.

Table 2
Isotopic ratios measured in Jupiter and Saturn.

Isotopic ratio	Jupiter			Saturn		
	η	$\Delta\eta$	Reference	η	$\Delta\eta$	Reference
D/H (in H_2)	2.60×10^{-5}	0.70×10^{-5}	Niemann et al. (1998)	1.70×10^{-5}	$^{+0.75}_{-0.45} \times 10^{-05}$	Lellouch et al. (2001)
				1.80×10^{-5}	$\pm 0.5 \times 10^{-05}$	Bézard et al. (2003)
$^3He/^4He$	1.66×10^{-4}	0.05×10^{-4}	Niemann et al. (1998)	–	–	
$^{12}C/^{13}C$ (in CH_4)	92.6	$^{+4.5}_{-4.1}$	Niemann et al. (1996)	91.8	$^{+8.4}_{-7.8}$	Fletcher et al. (2009b)
$^{14}N/^{15}N$ (in NH_3)	434.8	$^{+65}_{-50}$	Wong et al. (2004)	–	–	
$^{20}Ne/^{22}Ne$	13.0	2.0	Mahaffy et al. (2000)	–	–	
$^{36}Ar/^{38}Ar$	5.6	0.25	Mahaffy et al. (2000)	–	–	
^{128}Xe/total Xe	0.018	0.002	Atreya et al. (2003)	–	–	
^{129}Xe/total Xe	0.285	0.021	Atreya et al. (2003)	–	–	
^{130}Xe/total Xe	0.038	0.005	Atreya et al. (2003)	–	–	
^{131}Xe/total Xe	0.203	0.018	Atreya et al. (2003)	–	–	
^{132}Xe/total Xe	0.290	0.020	Atreya et al. (2003)	–	–	
^{134}Xe/total Xe	0.091	0.007	Atreya et al. (2003)	–	–	
^{136}Xe/total Xe	0.076	0.009	Atreya et al. (2003)	–	–	

Table 3
Enrichments in Jupiter and Saturn relatives to Protosun.

Species	Jupiter		Saturn	
	E	ΔE[a]	E	ΔE[a]
C	4.3	1.1	9.6	1.0
N	4.1	2.0	2.8	1.1
O[b]	0.4	0.1	1.6×10^{-4}	2.9×10^{-5}
P	3.3	0.4	11.2	1.3
S	2.9	0.7	12.05	–
He	0.8	0.0	0.7	0.1
Ne[c]	0.1	0.0	–	–
Ar	2.5	0.8	–	–
Kr	2.2	0.6	–	–
Xe	2.1	0.6	–	–

[a] Error is defined as $(\Delta E/E)^2 = (\Delta X/X_{planet})^2 + (\Delta X/X_{Protosun})^2$.

[b] This is a lower limit.

[c] This is an upper limit.

Table 4
Elemental abundances in the Sun and Protosun.

Element	Solar dex	Protosolar dex	Δdex	Protosolar X/H_2	$\Delta(X/H^2)$
C	8.39	8.44	0.04	5.55×10^{-04}	5.35×10^{-05}
N	7.86	7.91	0.12	1.64×10^{-04}	5.21×10^{-05}
O	8.73	8.78	0.07	1.21×10^{-03}	2.12×10^{-04}
P	5.46	5.51	0.04	6.52×10^{-07}	6.29×10^{-08}
S	7.14	7.19	0.01	3.12×10^{-05}	7.27×10^{-07}
He	10.93	10.99	0.02	1.94×10^{-01}	9.13×10^{-03}
Ne	8.05	8.10	0.10	2.54×10^{-04}	6.56×10^{-05}
Ar	6.50	6.55	0.10	7.15×10^{-06}	1.85×10^{-06}
Kr	3.28	3.33	0.08	4.31×10^{-09}	8.71×10^{-10}
Xe	2.27	2.32	0.08	4.21×10^{-10}	8.51×10^{-11}

Corrections for protosolar abundances ($+0.061$ dex (He) and $+0.053$ dex (others)) are taken from Lodders et al. (2009).

can provide useful constraints on Saturn's deep H_2O abundance. The upper tropospheric mole fraction of CO is representative of the H_2O abundance in the deep hot troposphere, where the two species are linked by the thermochemical equilibrium reaction (Fegley and Lodders, 1994):

$$H_2O + CH_4 = CO + 3H_2. \qquad (1)$$

It is thus possible to derive the deep H_2O abundance from CO observations using the "quench level" approximation (e.g., Bézard et al., 2002), or more rigorously using comprehensive thermo-chemical models (e.g., Visscher et al., 2010; Cavalié et al., 2014).

We have adapted the model of Venot et al. (2012) to Saturn's troposphere to assess the relevance of measuring CO with an in situ probe. The thermochemical kinetic network comes from the engine industry and was thoroughly validated for high temperatures and pressures. The tropospheric thermal profile has been constructed from a recent retrieval of the latitudinally resolved $T(P)$ structure
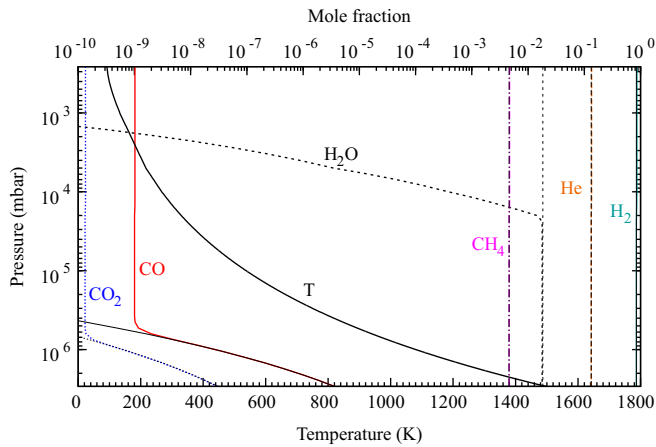
Fig. 1. Mole fraction profiles in the troposphere of Saturn obtained with Venot et al. (2012)'s model, targeting the 10^{-9} upper limit on the upper tropospheric CO mole fraction obtained by Cavalié et al. (2009). The temperature profile in the troposphere is shown in black solid line. Thermochemical equilibrium profiles are shown as black solid lines with the same layout as their corresponding species. The model parameters are O/H=21 times solar, C/H=9 times solar, and $K_{zz}=10^9$ cm² s⁻¹. Condensation of H_2O occurs around the 20 bar level in this model.

representing a mean of Cassini's prime mission (Fletcher et al., 2009b). We used the nominal mixing ratios from Table 1 for He and CH_4, and adopted an upper limit of 10^{-9} for CO (Cavalié et al., 2009). We have assumed a vertically constant eddy mixing coefficient K_{zz} ranging from 10^8 to 10^9 cm² s⁻¹ (Visscher et al., 2010). With $K_{zz}=10^8$ cm² s⁻¹, the deep atmospheric O/H ratio needs to be 62 times the protosolar value to reproduce the CO upper limit. With $K_{zz}=10^9$ cm² s⁻¹, the O/H still needs to be 18 times protosolar (see Fig. 1), i.e.., still much higher than Saturn's C/H ratio (9.9 times protosolar) but remains within the range of values predicted from the theory arguing that volatiles formed clathrates and pure condensates in the nebula (see Section 2.3.2). If we reversely set O/H ratio to the C/H one, then the most favorable case for a detection of CO ($K_{zz}=10^9$ cm² s⁻¹) gives an upper tropospheric mole fraction of CO of 4.1×10^{-10}. Reaching such a low value will remain very challenging for any ground-based facility. Besides, a complication comes from the fact that the observable CO vertical profile is largely dominated by an external source in the stratosphere (Cavalié et al., 2010).

These results argue in favor of an in situ measurement of tropospheric CO with a neutral mass spectrometer as a valuable complement to any attempt to directly measure the H_2O abundance. However, CO has a molecular weight very close to that of N_2. This degeneracy is a serious issue because the N_2 upper tropospheric mole fraction is expected to be around four orders of magnitude higher than the one of CO. A mass spectrometer will therefore need a mass resolution of $m/\Delta m = 2500$ to separate CO from N_2 at equal abundance, and about $m/\Delta m = 15,000$ for the CO and N_2 abundances expected in Saturn's atmosphere. More generally, any other disequilibrium species that reacts with H_2O, like PH_3 and SiH_4, is likely to provide additional constraints on the deep H_2O abundance of Saturn (Visscher and Fegley, 2005) and it would be desirable to include the combustion reaction schemes of such species (e.g., Twarowski, 1995; Miller et al., 2004) in thermochemical models.

2.3. Isotopic measurements at Saturn

As shown in Table 2, very little is known today concerning the isotopic ratios in Saturn's atmosphere. Only D/H (for H_2 and methane) and $^{12}C/^{13}C$ (for methane) ratios have been measured

so far (Lellouch et al., 2001; Bézard et al., 2003; Fletcher et al., 2009b).

The case of D/H is interesting and would deserve further measurements with smaller errors. Because deuterium is destroyed in stellar interiors and transformed into ^3He, the D/H value presently measured in Jupiter's atmosphere is estimated to be larger by some 5–10% than the protosolar value. This slight enrichment would have resulted from a mixing of nebular gas with deuterium-rich ices during the planet's formation, as suggested by Guillot (1999). For Saturn, the contribution of deuterium-rich ices in the present D/H ratio could be higher (25–40%). An accurate measurement of the D/H ratio in Saturn's atmosphere could provide, consequently, some constraints on the relative contribution of deuterium-rich ices during the formation of Saturn. Such a constraint is also based on the a priori knowledge of the protosolar D/H ratio, which remains relatively uncertain. This ratio is estimated from measurements of $^3He/^4He$ in the solar wind, which is corrected for changes that occurred in the solar corona and chromosphere subsequently to the evolution of the Sun's interior, and to which the primordial $^3He/^4He$ is subtracted. This latter value is estimated from the ratio observed in meteorites or in Jupiter's atmosphere. The measurement of $^3He/^4He$ in Saturn's atmosphere would also complement, consequently, the scientific impact of D/H measurement. In any case the smaller value of D/H measured by Lellouch et al. (2001) in Saturn's atmosphere from infrared spectra obtained by the Infrared Space Observatory (ISO) satellite and the Short Wavelength Spectrometer (SWS) compared to Jupiter's atmosphere (Niemann et al., 1998) is surprising in the sense that it would suggest a lower relative contribution of deuterium-rich ices in the formation of Saturn compared to Jupiter. These values have, nevertheless, large errors and so far no clear conclusion can be drawn.

The $^{14}N/^{15}N$ ratio presents large variations in the different planetary bodies in which it has been measured and, consequently, remains difficult to interpret. The analysis of Genesis solar wind samples (Marty et al., 2011) suggests a $^{14}N/^{15}N$ ratio of 441 ± 5, which agrees with the in situ measurements made in Jupiter's atmospheric ammonia (Fouchet et al., 2000, 2004) which probably comes from primordial N_2.[3] Terrestrial atmospheric N_2, with a value of 272, appears enriched in ^{15}N compared to Jupiter and similar to the bulk of ratios derived from the analysis of comet 81P/Wild 2 grains (McKeegan et al., 2006). Measurements performed in Titan's atmosphere, which is dominated by N_2 molecules, lead to 167.7 ± 0.6 and 147.5 ± 7.5 from the Cassini/INMS and Huygens/GCMS data, respectively (Niemann et al., 2010; Mandt et al., 2009). Because of the low abundance of primordial Ar observed by Huygens, it is generally assumed that N_2 is of secondary origin in Titan's atmosphere and that N was delivered in a less volatile form, probably NH_3. Different mechanisms have been proposed for the conversion of NH_3 to N_2. Isotopic fractionation may have occurred for nitrogen in Titan's atmosphere but the atmospheric model published by Mandt et al. (2009) suggests that the current $^{14}N/^{15}N$ ratio observed in N_2 is close to the value acquired by the primordial ammonia of Titan. This statement is supported by the recent measurement of the $^{14}N/^{15}N$ isotopic ratio in cometary ammonia (Rousselot et al., 2014). This ratio, comprised between 80 and 190, is consistent with the one measured in Titan.

---

[3] Thermochemical models predict the inhibition of the conversion of N_2 into NH_3 in the protosolar nebula, implying that N_2 was the main nitrogen-bearing molecule (Lewis and Prinn, 1980; Mousis et al., 2002). Moreover, the $^{14}N/^{15}N$ ratio in the solar wind has found identical to the value measured by the Galileo probe in Jupiter, indicating that the protosolar nitrogen present in the nebula also shared the same value (Marty et al., 2011). The fact that Jupiter accreted primordial N_2 is also found consistent with the other measurements of nitrogen isotopes in the solar system, Owen et al., 2001.

All these measurements suggest that N_2 and NH_3 result from the separation of nitrogen into at least two distinct reservoirs, with a distinct ^{15}N enrichment, which never equilibrated. The reservoir containing N_2 would have a large $^{14}N/^{15}N$ ratio (like in Jupiter's atmosphere, where the present ammonia is supposed to come from primordial N_2) and the one containing NH_3 a much lower value (like in Titan's atmosphere, where the present N_2 could come from primordial ammonia, and in cometary ammonia). In this context measuring $^{14}N/^{15}N$ in Saturn's atmosphere would be very helpful to get more information about the origin of ammonia in this planet.

The cases of carbon, oxygen and noble gases (Ne, Ar, Kr, and Xe) isotopic ratios are different because they should be representative of their primordial values. Only little variations are observed for the $^{12}C/^{13}C$ ratio in the solar system irrespective of the body and molecule in which it has been measured. This ratio appears compatible with the terrestrial value of 89 (except if isotopic fractionation processes occur, like for methane in Titan, but the influence of these processes on this ratio is small). Table 2 provides the value of 91.8 measured by Fletcher et al. (2009b) in Saturn with the Cassini/CIRS but with large error bars. A new in situ measurement of this ratio should be useful to confirm that carbon in Saturn is also representative of the protosolar value (and different from the one present in the local Interstellar Medium (ISM) because ^{13}C is created in stars). The oxygen isotopic ratios also constitute interesting measurements to be made in Saturn's atmosphere. The terrestrial $^{16}O/^{18}O$ and $^{16}O/^{17}O$ isotopic ratios are 499 and 2632, respectively (Asplund et al., 2009). At the high accuracy levels possible with meteorites analysis these ratios present some small variations.[4] Measurements performed for solar system objects like comets, far less accurate, match the terrestrial $^{16}O/^{18}O$ value (with error bars being typically a few tens). However no $^{16}O/^{18}O$ ratio has been yet published for Saturn's atmosphere. The only $^{16}O/^{18}O$ measurement made so far for a giant planet (Noll et al., 1995) was obtained from ground-based IR observations in Jupiter's atmosphere and had a very large uncertainty (1–3 times the terrestrial value).

2.4. Interpretations of the volatile enrichments in Jupiter and Saturn

Several theories connecting the thermodynamic evolution of the protosolar nebula to the formation conditions of the giant planets have been developed to interpret the volatile enrichments measured in Jupiter and Saturn. The main scenarios proposed in the literature and their predictions for Saturn's composition are summarized below.

2.4.1. Amorphous ice scenario

The model proposed by Owen et al. (1999) is the first attempt to explain the volatile enrichments measured in Jupiter's atmosphere. In this scenario, the basic assumption is that volatiles present in Jupiter's atmosphere were trapped in amorphous ice in the protosolar nebula. In this model, amorphous ices originated from ISM and survived the formation of the protosolar nebula. This is the fraction of the icy planetesimals that vaporized when entering the envelope of the growing Jupiter, which engendered the observed volatile enrichments. If correct, this scenario predicts that the volatiles (O, C, N, S, Ar, Kr and Xe) should be enriched by a similar factor in Saturn's atmosphere, as seems to be the case for Jupiter, given the size of the error bars of measurements. In this case, comets as well as Kuiper Belt Objects, would have also been accreted from amorphous ice.

---

[4] Expressed in δ units, which are deviations in part per thousand, they are typically a few units.

2.4.2. Crystalline ice scenario

An alternative interpretation of the volatile enrichments measured in Jupiter is the one proposed by Gautier et al. (2001) and subsequent papers by Hersant et al. (2004), Gautier and Hersant (2005), Alibert et al. (2005a) and Mousis et al. (2006). This interpretation is based on the analysis made by Kouchi et al. (1994), which shows that water condenses in the form of crystalline ice at ~ 150 K in the conditions occurring in the protosolar nebula. In this scenario, water vapor crystallized and trapped the volatiles in the form of clathrates or hydrates (case of NH_3) in the 40–90 K range instead of condensing at lower temperatures. The case of CO_2 is specific because this species condenses at relatively high temperature. All ices then agglomerated and formed the planetesimals that were ultimately accreted by the growing Jupiter. However, the theory of the trapping by clathration is subtle since it occurs in a cooling nebula and consumes water ice. Once ice is consumed, clathration stops. Aforementioned works postulate that the amount of available crystalline water ice was large enough (typically $H_2O/H_2 \geq 2 \times (O/H)_\odot$) to trap the other volatiles in the feeding zone of Jupiter and that the disk's temperature at which the ices formed never decreased below ~ 40 K. The volatile enrichments in Jupiter can also be explained via the accretion and the vaporization in its envelope of icy planetesimals made from a mixture of clathrates and pure condensates (Mousis et al., 2009, 2012). These planetesimals could have formed if the initial disk's gas phase composition was fully protosolar (including oxygen), and if the disk's temperature decreased down to ~ 20 K at their formation location. In all these scenarios, the building blocks of giant planets, their satellite systems, comets and Kuiper Belt Objects would have been agglomerated from a mixture of clathrates, hydrates and pure condensates with proportions determined from (i) the abundance of crystalline ice available at the trapping epoch of volatiles and (ii) the lowest temperature reached by the cooling protosolar nebula prior to its dissipation.

The model described in Mousis et al. (2009, 2012) is used here to show fits of the volatile enrichments measured at Jupiter and Saturn, which have been updated by using the recent protosolar abundances of Lodders et al. (2009) (see Table 3). This model is used to compute the composition of planetesimals condensed from two extreme gas phase compositions of the nebula, namely oxidizing (composition usually assumed for the protosolar nebula) and reducing states (see Johnson et al., 2012 for a full description of the used disk's gas phase compositions). Planetesimals formed during the cooling of the nebula from these two extreme gas phase compositions are assumed to have been accreted by proto-Jupiter and proto-Saturn and devolatilized in the envelopes during their growth phases. Once the composition of the planetesimals is defined, the adjustment of their masses accreted in the envelopes of Jupiter and Saturn allows one to determine the best fit of the observed volatile enrichments. In the two cases, the abundance of available crystalline water is derived from protosolar O and the disk is assumed to cool down to ~ 20 K.

Figs. 2 and 3 represent the fits of the enrichments observed in Jupiter's and Saturn's atmospheres, respectively. In the case of Jupiter, C, N, S, Ar and Kr measurements are matched by our fits, irrespective of the redox status of the protosolar nebula. Also, in both redox cases, the measured P abundance is not matched by the fits but this might be due to the difficulty of getting a reliable measurement since the mid-infrared spectrum is dominated by tropospheric ammonia. On the other hand, Xe is almost matched by our fit in the reducing case only. The oxygen abundance is predicted to be 5.3–5.7 and 6.2–7.8 times protosolar in Jupiter in the oxidizing and reducing cases, respectively.

In the case of Saturn, the strategy was to fit the measured C enrichment. Interestingly, contrary to Jupiter, P is matched in Saturn, irrespective of the redox status of the nebula. On the other hand, the P determination is more robust in Saturn than in Jupiter
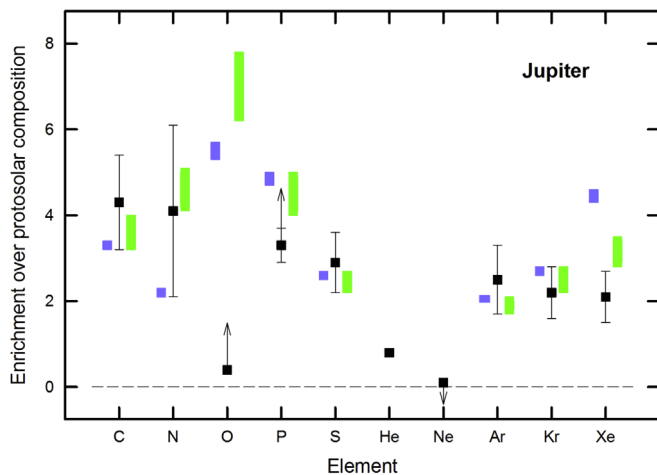
Fig. 2. Ratio of Jovian to protosolar abundances. Black squares and black bars correspond to measurements and their associated uncertainties. Blue and green bars correspond to calculations assuming oxidizing and reducing conditions in the protosolar nebula, respectively (see text). Arrows pointing up correspond to the possibility that the measured oxygen and phosphorus abundances are lower than their bulk abundances, and arrow pointing down to the fact that the measured Ne abundance is an upper limit. (For interpretation of the references to color in this figure caption, the reader is referred to the web version of this paper.)
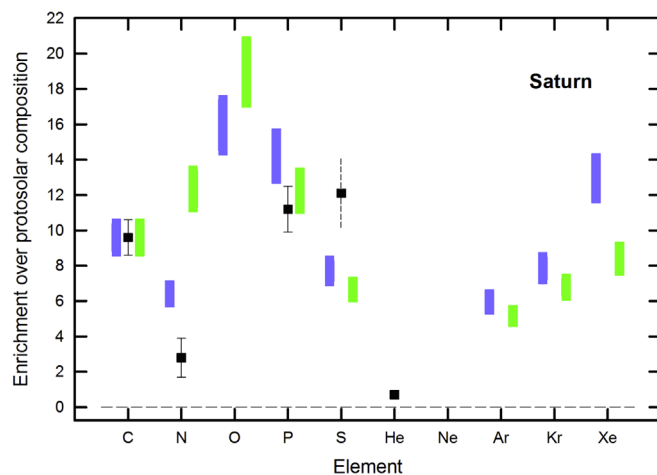

Fig. 3. Ratio of Saturnian to protosolar abundances. Black squares and black bars correspond to measurements and their associated uncertainties. The O value measured in the troposphere would be close to zero on the utilized scale. Blue and green bars correspond to calculations assuming oxidizing and reducing conditions in the protosolar nebula, respectively (see text). (For interpretation of the references to color in this figure caption, the reader is referred to the web version of this paper.)

because PH_3 dominates the mid-infrared spectrum. However, S is not matched by our model but this might result from the lack of reliability of its determination. In addition, with enrichments predicted to be ~ 5.7–7.1 times and 11.1–13.6 times the protosolar value in the oxidizing and reducing cases, respectively, our model overestimates the amount of nitrogen present in Saturn's atmosphere compared to observations that suggest a more moderate enrichment, in the order of ~ 1.7–3.9 times the protosolar value. One possibility that could explain this discrepancy is that all NH_3 and only a fraction of N_2, this latter being the most abundant N-bearing volatile in the protosolar nebula (Lewis and Prinn, 1980), would have been incorporated in Saturn's building blocks because of the limited amount of available water favoring its trapping efficiency in clathrates. The remaining fraction of N_2 would have remained in the H_2-dominated gas phase of Saturn's feeding zone as a result of the disk's cooling down to temperatures higher than

that of N_2 condensation or trapping in clathrates, as proposed by Hersant et al. (2008). These conditions could lead to a moderate N enrichment comparable to the measured one and to a $^{14}N/^{15}N$ ratio in the envelope lower than the Jovian value. In this case, the abundances of Ar and Kr would remain protosolar because the disk never cooled down enough to enable the condensation of these two species. In contrast, because the disk is assumed to cool down to very low temperatures at Saturn's formation location, our model predicts Ar, Kr and Xe enrichments in the two redox cases. In addition, the oxygen abundance is predicted to be 14.3–17.6 and 17–20.9 times protosolar in the oxidizing and reducing cases, respectively.

2.4.3. Scenario of supply of refractory carbonated material

Lodders (2004) proposed the formation of Jupiter from refractory carbonated materials, namely "tar", placing its formation location on a "tar line" in the protosolar nebula. This scenario was used to explain the elemental abundances enrichments observed by Galileo after having normalized all the heavy elements' abundances with respect to Si instead of H_2. By doing so, Lodders (2004) found that the relative abundances of Ar, Kr, Xe and P are solar, C and possibly N are enriched, and H, He, Ne, and O are subsolar, with the Galileo H_2O determination assumed to be representative of the planet's bulk O/H. In this model, Ar, Kr and Xe would have been supplied to Jupiter via direct gravitational capture of the solar nebula gas. To explain the Ar, Kr and Xe enrichments in the Jovian atmosphere, Lodders (2004) proposed that they would have been the consequence of the H_2 and He depletion in the envelope, which produced the metallic layer. If Saturn formed following this scenario, a useful test would be the determination of the H_2O bulk abundance, which should be subsolar, as proposed by Lodders (2004) for Jupiter.

2.4.4. Scenario of disk's gas phase enrichment

To account for the enrichments in heavy noble gases observed in Jupiter's atmosphere, Guillot and Hueso (2006) proposed that Ar, Kr and Xe have condensed at ~ 20–30 K onto the icy amorphous grains that settled in the cold outer part of the disk nebula midplane. These noble gases would have been released in gaseous form in the formation region of giant planets at a time when the disk would have been chemically evolved due to photoevaporation. The combination of these mechanisms would have led to a heavy noble gas enrichment relative to protosolar in the disk's gas phase from which the giant planets would have been accreted. In Guillot and Hueso (2006)'s scenario, the noble gas enrichment would have been homogeneous in the giant planets formation region. Therefore, their model predicts that the Ar, Kr and Xe enrichments in Saturn's atmosphere are similar to those observed in Jupiter, which are between ~ 1.5 and 3.3 times the protosolar value (see Table 3). These values are substantially smaller than those predicted by the model used in Section 2.4.2, which are in the ~ 4.6–14.3 times protosolar range, depending on the considered species (see Fig. 3).

2.5. Summary of key measurements

Here we provide the measurements in Saturn's atmosphere achievable down to the 10 bar limit and that would allow disentangling between the aforementioned giant planets formation scenarios:

- The atmospheric fraction of He/H_2 with a 2% accuracy on the measurement (the same accuracy as the one made by the Jamin–Mascart interferometer aboard Galileo).

- The elemental enrichments in cosmogenically abundant species C, N and S. C/H, N/H and S/H should be sampled with an accuracy better than $\pm\,10\%$ (uncertainties of the order of protosolar abundances).
- The elemental enrichments in minor species delivered by vertical mixing (*e.g.*, P, As, Ge) from the deeper troposphere (see also Section 3). P/H, As/H and Ge/H should be sampled with an accuracy better than $\pm\,10\%$ (uncertainties of the order of protosolar abundances).
- The isotopic ratios in hydrogen (D/H), oxygen (^{18}O, ^{17}O and ^{16}O), carbon ($^{13}C/^{12}C$) and nitrogen ($^{15}N/^{14}N$), to determine the key reservoirs for these species (*e.g.*, delivery as N_2 or NH_3 vastly alters the $^{15}N/^{14}N$ ratio in the giant planet's envelope). $^{13}C/^{12}C$, $^{18}O/^{16}O$ and $^{17}O/^{16}O$ should be sampled with an accuracy better than $\pm\,1\%$. D/H, $^{15}N/^{14}N$ should be analyzed in the main host molecules with an accuracy of the order of $\pm\,5\%$.
- The abundances and isotopic ratios for the chemically inert noble gases He, Ne, Xe, Kr and Ar provide excellent tracers for the materials in the subreservoirs existing in the protosolar nebula. The isotopic ratios for He, Ne, Xe, Kr and Ar should be measured with an accuracy better than $\pm\,1\%$.

The depth of probe penetration will determine whether it can access the well-mixed regions for key condensable volatiles. In the case of Saturn, a shallow probe penetrating down to $\sim$10 bar would *in principle* sample ammonia and H_2S both within and below their cloud bases, in the well-mixed regions of the atmosphere to determine the N/H and S/H ratios, in addition to noble gases and isotopic ratios. Note that the N determination could be a lower limit because ammonia is highly soluble in liquid water. Rain generated in the water cloud can provide a downward transport mechanism for ammonia, so the ammonia abundance above the water cloud could be less than the bulk abundance. Because the hypothesized water cloud is deeper than at least $\sim$12.6 bar in Saturn (Atreya et al., 1999), the prospect of reaching the deep O/H ratio remains unlikely if the probe would not survive beyond its design limit, unless a precise determination of the CO abundance (or any other species limited by reactions with the tropospheric water) is used to constrain H_2O/H_2 (see Section 2.2) and/or the probe is accompanied by remote sensing experiments on a carrier spacecraft capable of probing these depths (*e.g.*, the Juno microwave radiometer, currently en route to Jupiter). Nevertheless, measuring elemental abundances (in particular He, noble gases and other cosmogenically common species) and isotopic ratios using a shallow entry probe on Saturn will provide a vital comparison to Galileo's measurements of Jupiter, and a crucial "ground-truth" for the remote sensing investigations by the Cassini spacecraft.

3. *In situ* studies of Saturn's atmospheric phenomena

The giant planets are natural planetary-scale laboratories for the study of fluid dynamics without the complicating influences of terrestrial topography or ocean–atmosphere coupling. However, remote sensing only provides access to limited altitude ranges where spectral lines are formed and broadened, typically from the cloud-forming weather layer upwards into the middle atmosphere, although deep-sounding at microwave wavelengths can probe through the upper cloud decks. Furthermore, the vertical resolution of "nadir" remote sensing is fundamentally limited to the width of the contribution function (*i.e.*., the range of altitudes contributing to the upwelling radiance at a given wavelength), which can extend over one or more scale heights. Ground-based observatories, space telescopes and the visiting Pioneer, Voyager and Cassini missions have exploited wavelengths from the

ultraviolet to the microwave in an attempt to reconstruct Saturn's atmospheric structure in three dimensions. These studies have a limited vertical resolution and principally use visible and infrared observations in the upper troposphere (just above the condensate clouds and within the tropospheric hazes) or the mid-stratosphere near the 1 mbar level via mid-infrared emissions. Regions below the top-most clouds and in the middle/upper atmosphere are largely inaccessible to remote sensing, limiting our knowledge of the vertical variations of temperatures, densities, horizontal and vertical winds and waves, compositional profiles and cloud/haze properties. Nevertheless, remote sensing has proven invaluable in determining the horizontal and temporal variability of Saturn's temperatures, winds, composition and cloud properties, providing the global context that will prove essential in interpreting probe results, as they did for the Galileo probe. *In situ* exploration of Saturn would not only help constrain the bulk chemical composition of this gas giant (*e.g.*, Section 2), but it would also provide direct sampling and "ground-truth" for the myriad physical and chemical processes at work in Saturn's atmosphere.

In the following sections we describe how an *in situ* probe, penetrating from the upper atmosphere (μ bar pressures) into the convective weather layer to a minimum depth of 10 bar, would contribute to our knowledge of Saturn's atmospheric structure, dynamics, composition, chemistry and cloud-forming processes. These results would be directly compared to our only other direct measurement of a giant planet, from the descent of the 339-kg Galileo probe into the atmosphere of Jupiter on December 7, 1995. The Galileo probe entered a region of unusual atmospheric dynamics near 6.5°N, where it is thought that the meteorology associated with planetary wave activity conspired to deplete Jupiter's atmosphere in volatiles (*e.g.*, Showman and Dowling, 2000; Friedson, 1999), most notably preventing the probe from reaching the depth of Jupiter's well-mixed H_2O layer after its 60-min descent to the 22 bar level, 150 km below the visible cloud-tops. In the decade that followed, researchers have been attempting to reconcile global remote sensing of Jupiter with this single-point measurement (*e.g.*, Roos-Serote et al., 2000). Along with the GPMS and HAD instruments, the probe carried a net flux radiometer for the thermal profile and heat budget (NFR, Sromovsky et al., 1998); a nephelometer for cloud studies (NEP, Ragent et al., 1998) and an Atmospheric Structure Instrument (ASI, Seiff et al., 1998) to measure profiles of temperature, pressure and atmospheric density. Measurements of the probe's transmitted radio signal (driven by an ultra-stable oscillator) allowed a reconstruction of the zonal winds with altitude (Doppler Wind Experiment, DWE, Atkinson et al., 1998), and attenuation of the probe-to-orbiter signal also provided information on the microwave opacity due to ammonia absorption (Folkner et al., 1998). Comparable *in situ* data for Saturn, in tandem with the wealth of remotely sensed observations provided by Cassini, would enable a similar leap in our understanding of the solar system's second giant planet. Finally, from the perspective of comparative planetology, improving our understanding of Saturn will provide a valuable new context for Galileo probe's measurements at Jupiter, enhancing our knowledge of this unique class of planets.

3.1. Saturn's dynamics and meteorology

Saturn's atmosphere stands in contrast to Jupiter, with fewer large-scale vortices and a more subdued banded structure in the visible, superimposed onto hemispheric asymmetries in temperatures, cloud cover and gaseous composition as a result of Saturn's seasonal cycles (unlike Jupiter, Saturn has a considerable axial tilt of 26°). See West et al. (2009), Fouchet et al. (2009), Del Genio et al. (2009) and Nagy et al. (2009) for detailed reviews. Despite this globally variable atmosphere in the horizontal, a single entry

probe would provide unique insights in the vertical dimension by characterizing the changing environmental conditions and dynamical state as it descends from the stably stratified middle atmosphere to the convectively unstable troposphere. Although *in situ* probes may seem to provide one-dimensional vertical results, a horizontal dimension is also provided by Doppler tracking of the probe trajectory during its descent, as it is buffeted by Saturn's powerful jet streams and eddies.

3.1.1. Atmospheric stability and transition zones

A descending probe would primarily measure the vertical stability of the atmosphere, which reveals where the atmosphere transitions from statically stable (*e.g.*, the stratosphere and upper troposphere) to being unstable to convective motions (*e.g.*, the cloud-forming region). The *Brunt Väisälä* frequency, or buoyancy frequency, is related to the difference between the measured lapse rate and the dry adiabat, given by

$$N_B^2 = \frac{g}{T}\left(\frac{dT}{dz} + \frac{g}{C_p}\right) \qquad (2)$$

where g is the gravitational acceleration, C_p is the specific heat capacity and g/C_p is the dry adiabatic lapse rate. Positive buoyancy frequencies indicate static stability whereas negative frequencies indicate unstable conditions. This is further encapsulated in the dimensionless Richardson Number (Ri), which characterizes the dominant modes of instability in an atmospheric flow and measures the importance of the atmospheric stability against vertical shears on the zonal (u) and meridional (v) winds:

$$Ri = \frac{N_B^2}{\left(\frac{\partial u}{\partial z}\right)^2 + \left(\frac{\partial v}{\partial z}\right)^2} = \frac{\frac{g}{\theta}\left(\frac{\partial \theta}{\partial z}\right)}{\left(\frac{\partial u}{\partial z}\right)^2 + \left(\frac{\partial v}{\partial z}\right)^2} \qquad (3)$$

where θ is the potential temperature and $\partial\theta/\partial z$ the static stability. An entry probe can measure continuous profiles of the temperature profile, buoyancy frequency and static stability as a function of altitude, enabling a study of stability and instability regimes as a function of depth and identifying the dominant instability mechanisms via the Richardson number. Temperatures and densities in the upper atmosphere can be determined via the deceleration caused by atmospheric drag, connecting the high temperature thermosphere at nanobar pressures to the middle atmosphere at microbar and millibar pressures (*e.g.*, Yelle and Miller, 2004). An atmospheric structure instrument would measure atmospheric pressures and temperatures throughout the descent to the clouds, and from these infer atmospheric stability and densities (provided the mean molecular weight is determined by another instrument; Seiff et al., 1998; Magalhães et al., 2002). Upper atmospheric densities would be deduced from measured accelerations and from area and drag coefficients.[5] The probe will sample both the radiatively cooled upper atmosphere and also the convectively driven troposphere, precisely constraining the static stability, radiative–convective boundary (*i.e.*, how far down does sunlight penetrate?) and the levels of the tropopause, stratopause, mesopause and homopause. Thermal structure measurements of Saturn would be directly compared to those on Jupiter to understand the energetic balance between solar heating, thermal cooling, latent heat release, wave heating and internal energy for driving the complex dynamics of all the different atmospheric layers on the giant planets, and how this balance differs as a function of distance from the Sun.

3.1.2. Wave activity

Perturbations of the temperature structure due to vertical propagation of gravity waves are expected to be common features of the stably stratified middle atmospheres either on terrestrial planets or gas giants. Wave activity is thought to be a key coupling mechanism between the convective troposphere (*e.g.*, gravity waves and Rossby/planetary waves generated by rising plumes and vortices) and the stable middle/upper atmosphere, being responsible for transporting energy and momentum through the atmosphere and for phenomenon like the Quasi-Biennal Oscillation on Earth (Baldwin et al., 2001), which is thought to have counterparts on Jupiter and Saturn (Fouchet et al., 2008). Waves are a useful diagnostic of the background state of the atmosphere, as their propagation relies on certain critical conditions (*e.g.*, the static stability and vertical shears on zonal winds, which cannot be revealed by remote sensing alone). Energy and momentum transfer via waves serve as a source of both heating and cooling for the hot thermospheres, whose temperatures far exceed the expectations from solar heating alone, although the precise origins of the heating source have never been satisfactorily identified (*e.g.*, Hickey et al., 2000; Nagy et al., 2009). Although a probe at a single entry point cannot necessarily distinguish between wave types, nor measure the horizontal wavelength, it can measure the vertical wavelength of middle atmospheric waves. For example, the periodicity of gravity waves measured by the Galileo probe on Jupiter permitted the reconstruction of the zonal wind profile from the lower thermosphere to the upper troposphere (Watkins and Cho, 2013), and identification of the homopause (where molecular and eddy diffusion become comparable and gravity waves break to deposit their energy), above which the atmosphere separates into layers of different molecular species. Understanding the propagation, periodicity and sources of wave activity on Saturn will reveal the properties of the background medium and the coupling of the "weather layer" to the middle atmosphere especially on how zonal and meridional circulations are forced by eddy-mean flow interactions, and facilitate direct comparison with Jupiter.

3.1.3. Profiling atmospheric winds

In situ exploration would tackle one of the most enduring mysteries for the giant planets – What powers and maintains the zonal winds responsible for the planetary banding, how deep do those winds penetrate into the troposphere, and what are the wind strengths in the middle atmosphere? Remote sensing of temperature contrasts (and hence wind shears via thermal wind relationships) can reveal the slow overturning of the stratosphere, and inferences about the deep winds can be made from the properties of atmospheric plumes at the cloud-tops (*e.g.*, Sánchez-Lavega et al., 2008). However, remotely observed cloud motions are often ambiguous due to uncertainties in the cloud location; the clouds themselves may be imperfect tracers of the winds; and vertical temperature profiles (and hence wind shears) are degenerate with the atmospheric composition. *In situ* measurements of the vertical variation of winds, temperatures and cloud locations may help to resolve these ambiguities. The Galileo probe's DWE reported that jovian winds were at a minimum at the cloud tops (where most of our understanding of zonal winds and eddy-momentum fluxes originate from), and increased both above (Watkins and Cho, 2013) and below (Atkinson et al., 1998) this level. In the deep atmosphere, DWE demonstrated that Jupiter's winds increased to a depth of around 5 bar, and then remained roughly constant to the maximum probe depth of around 22 bar. Similar measurements on Saturn could sample the transition region between two different circulation regimes – an upper tropospheric region where eddies cause friction to decelerate the zonal jets and air rises in cloudy zones, and a deeper tropospheric region where the circulation is reversed and eddy pumping is essential to maintain the jets and air rises in the warmer belts (*e.g.*,

---

[5] Note that ablation sensors on the entry probe are needed to get the time-profile of Thermal Protection System (TPS) mass loss and change in area during entry.

Del Genio et al., 2009; Fletcher et al., 2011). A single entry probe would potentially sample both regimes, and reconciling these two views of tropospheric circulation on Saturn would have implications for all of the giant planets. Finally, direct measurements of winds in the middle atmosphere would establish the reliability of extrapolations from the jets in the cloud tops to the stratosphere in determining the general circulations of planetary stratospheres.

3.2. Saturn's clouds and composition

In Section 2 we discussed the need for reliable measurements of bulk elemental enrichments and isotopic ratios to study the formation and evolution of Saturn. Vertical profiles of atmospheric composition (both molecular and particulate) are essential to understanding the chemical, condensation and disequilibrium processes at work, in addition to the deposition of material from outside of the planet's atmosphere. The Galileo probe compositional and cloud measurements revealed an unexpectedly dry region of the jovian troposphere, depleted in clouds and volatiles (Atreya et al., 1999), which was consistent with ground-based observations of the probe entry into a warm cyclonic region (e.g., Orton et al., 1998). For this reason, the compositional profiles measured by Galileo are not thought to be globally representative of Jupiter's atmosphere, leading to a desire for multiple entry probes for different latitudes and longitudes in future missions. Nevertheless, a single probe is essential for a more complete understanding of this class of giant planets, to enhance our knowledge of Saturn and to provide a context for improved interpretation of the Galileo probe's sampling of Jupiter's unusual meteorology.

3.2.1. Clouds and hazes

A poor understanding of cloud and haze formation in planetary atmospheres of our solar system may be the key parameter limiting our ability to interpret spectra of extrasolar planets and brown dwarfs (e.g., Marley et al., 2013). Although equilibrium cloud condensation models (ECCMs, Weidenschilling and Lewis, 1973) combined with the sedimentation of condensates to form layers have proven successful in explaining the broad characteristics of the planets (methane ice clouds on ice giants, ammonia ice clouds on gas giants), they remain too simplistic to reproduce the precise location, extent and microphysics of the observed cloud decks. The Galileo probe results defied expectations of equilibrium condensation by revealing clouds bases at 0.5, 1.3 and 1.6 bar, plus tenuous structure from 2.4 to 3.6 bar and no evidence for a deep water cloud (Atreya et al., 1999; West et al., 2004). Ammonia ice on Jupiter has only been spectroscopically identified in regions of powerful convective updrafts (e.g., Baines et al., 2002; Reuter et al., 2007), and water ice has been detected in Voyager far-infrared spectroscopy (Simon-Miller et al., 2000). The spectral signature of pure ammonia ice is likely obscured by a coating or mixing with other products, such as photolytically produced hydrocarbons, hydrazine or diphosphine (e.g., Sromovsky and Fry, 2010; West et al., 2004). The spectral properties of these mixtures are poorly known, rendering cloud remote sensing highly ambiguous. Furthermore, Saturn's upper troposphere appears dominated by a ubiquitous haze whose composition has never been determined and is potentially unrelated to condensed volatiles (although diphosphine, P_2H_4, a product of the UV destruction of phosphine, remains an intriguing possibility). An ECCM applied to Saturn with a $5 \times$ enhancement of heavy elements over solar abundances predicts NH_3 condensation at 1.8 bar, NH_4SH near 4 bar and an aqueous ammonia cloud (merging with a water ice cloud) near 20 bar (Atreya et al., 1999). However, ammonia and water ice signatures have been identified

only recently, in the powerful updrafts associated with a powerful springtime storm in 2010–2011 (Sromovsky et al., 2013).

The only way to resolve these questions is by in situ sampling of the clouds and hazes formed in a planet's atmosphere, using instruments designed to measure the particle optical properties, size distributions, number and mass densities, optical depth and vertical distribution. Combined with the vertical profiles of condensable volatiles (e.g., NH_3, H_2S and H_2O on Saturn) and photochemically produced species (hydrocarbons, hydrazine N_2H_4, diphosphine), this would give an estimate of the composition of Saturn's condensation clouds and upper atmospheric hazes for the first time. Saturn's atmosphere provides the most accessible cloud decks for this study after Jupiter (condensates of NH_3 and H_2O are locked away at considerably higher pressures on the ice giants); the most useful comparison to remote sensing data (e.g., from Cassini); and the most similar composition to Jupiter for a full understanding of gas giant clouds.

Furthermore, the in situ exploration of a giant planet weather layer will provide new insights into the cloud-forming processes and the dynamics below the levels normally visible to remote sensing. Lightning flashes most likely exist in the atmospheres of all gas planets (Yair et al., 2008), and the Galileo Probe lightning and radio emission detector (LRD) used a magnetic antenna to detect signals of lightning from Jovian clouds with an electric dipole moment change about 100 times that of terrestrial lightning (Rinnert et al., 1998). The existence of lightning in Saturn's atmosphere has been proven by Voyager and Cassini measurements of radio emissions (Fischer et al., 2008) and direct optical flash observations (Dyudina et al., 2010). The thunderstorms tend to appear infrequently at the equator and in the "storm alleys" at the latitudes of 35° north and south. The flashes originate from a depth of 125–250 km below the 1-bar level, most likely in the water clouds. So far, Saturn lightning radio emissions have only been measured above the ionospheric cutoff frequency (mostly > 1 MHz). Measurements in the VLF region (3–30 kHz) can reveal the unknown spectrum at lower frequencies, where lightning radio emissions are expected to be strongest and to be able to propagate over thousands of kilometers below the ionosphere. Another unique and new measurement for gas planets concerns Schumann resonances in the TLF (< 3 Hz) and ELF regions (3–300 Hz), which should be excited by lightning in their gaseous envelopes (e.g., Sentman, 1990). It has been suggested that such a measurement could even constrain the water abundance on giant planets (Simões et al., 2012), and it would be very useful in conjunction with conductivity measurements throughout the descent of the probe.

3.2.2. Atmospheric chemistry and mixing

Gaseous species can be removed from the gas phase by condensation; modified by vertical mixing and photolysis; and deposited from exogenic sources (icy rings, satellites, interplanetary dust, comets, etc.), causing abundance profiles to vary with altitude and season. Indeed, all the giant planets exhibit a rich chemistry due to the UV photolysis of key atmospheric species. Their stratospheres are dominated by the hydrocarbon products of methane photolysis (e.g., Moses et al., 2005), which descend into the troposphere to be recycled by thermochemical conversion. On Jupiter, the Galileo probe was able to measure hydrocarbon species in the 8–12 bar region, although the balance of ethane (expected to be the most abundant hydrocarbon after methane) to ethylene, propene, acetylene and propane led to suspicions that the hydrocarbon detections were instrumental rather than of atmospheric origin (Wong, 2009). Stratospheric measurements of hydrocarbons in their production region were not performed, but would be possible on Saturn with a probe. Saturn's troposphere

features saturated volatiles in trace amounts above the cloud tops, but only ammonia gas is abundant enough for remote detection. H_2S and H_2O profiles above the condensation clouds have never been measured. In addition to the volatiles, Saturn's troposphere features a host of disequilibrium species, most notably phosphine, dredged up from the deeper, warmer interior by vigorous atmospheric mixing (e.g., Fletcher et al., 2009a). The abundance of PH_3 measured in the upper troposphere is thought to represent the abundance at its thermochemical quench level, where the vertical diffusion timescale is shorter than the thermochemical kinetics timescale. Measurements of additional trace species in the troposphere (GeH_4, AsH_3, CO) provide constraints on the strength of atmospheric mixing from deeper, warmer levels below the clouds. CO is of particular interest because it could be used as a probe of the deep O/H ratio of Saturn (see Section 2).

Detection of trace chemical species (HCN, HCP, CS, methanol, formaldehyde) and hydrogen halides (HCl, HBr, HF and HI, e.g., Teanby et al., 2006; Fletcher et al., 2012) would reveal coupled chemistry due to lightning activity or shock chemistry due to planetary impacts. In addition, the presence of oxygenated species in the upper stratosphere (CO, CO_2, H_2O) reveal the strength of exogenic influx of materials (comets, interplanetary dust, e.g., Feuchtgruber et al., 1997; Cavalié et al., 2010) into the upper atmosphere of Saturn. Sensitive mass spectrometry of these species, combined with probe measurements of atmospheric temperatures and haze properties, could reveal the processes governing the soup of atmospheric constituents on the giant planets. Once again, Saturn's trace species are expected to be the most accessible of the solar system giant after Jupiter, as volatiles and disequilibrium species (e.g., PH_3 and NH_3) have so far eluded remote detection on the ice giants.

3.3. Summary of key atmospheric measurements

A single entry probe would reveal new insights into the vertical structures of temperatures, density, chemical composition and clouds during descent through a number of different atmospheric regions, from the stable upper/middle atmosphere to the convective troposphere. It would directly sample the condensation cloud decks and ubiquitous hazes whose composition, altitude and structure remain ambiguous due to the inherent difficulties with remote sensing. Furthermore, it would show how Saturn's atmosphere flows at a variety of different depths above, within and below the condensate clouds. Key measurements required to address the science described in this section include:

- Continuous measurements of atmospheric temperature and pressure throughout the descent to study (i) stability regimes as a function of depth though transition zones (e.g., radiative–convective boundary); (ii) atmospheric drag and accelerations; and (iii) the influence of wave perturbations and cloud formation on the vertical temperature profile.
- Determination of the vertical variation of horizontal winds using Doppler measurements of the probe's carrier frequency (driven by an ultra-stable oscillator) during the descent. This includes a study of the depth of the zonal wind fields, as well as the first measurements of middle atmospheric winds.
- Vertical profiling of a host of atmospheric species via mass spectrometry, including atmospheric volatiles (water, H_2S and NH_3 in their saturated and sub-cloud regions); disequilibrium species (e.g., PH_3, AsH_3, GeH_4, CO) dredged from the deeper atmosphere; photochemical species (e.g., hydrocarbons and HCN in the troposphere and stratosphere; hydrazine and diphosphine in the upper troposphere) and exogenic inputs (e.g., oxygenated species in the upper atmosphere).

- Measurements of the vertical structure and properties of Saturn's cloud and haze layers; including determinations of the particle optical properties, size distributions, number and mass densities, opacity, shapes and, potentially, their composition.

With a single entry probe, the selected entry site must be carefully studied. Saturn's equatorial zone is one potential site for a single entry probe because of its meteorological activity that combines: the emergence of large-scale storms (Sanchez-Lavega et al., 1991); vertical wind shears in the troposphere (García-Melendo et al., 2011); upwelling enhancing volatiles and disequilibrium species (Fletcher et al., 2009a, 2011); and a global stratospheric oscillation of the thermal field (Fouchet et al., 2008; Orton et al., 2008; Guerlet et al., 2011). Additionally, the strength of its equatorial eastward jet (peak velocities up to 500 m/s) poses one of the theoretical challenges to the understanding of the dynamics of fluid giant planets. Furthermore, a descent probe into Saturn's equatorial region could further constrain the influx of H_2O originating from the Enceladus torus (Hartogh et al., 2011). However, it remains an open question as to how representative the equatorial region would be of Saturn's global dynamics. Short of multiple entry probes targeted at different regions of upwelling and subsidence, near to narrow prograde jets or broader retrograde jets, a mid-latitude atmospheric region might be a more representative sample.

4. Mission architectures

The primary science objectives described in Sections 2 and 3 may be addressed by an atmospheric entry probe that would descend under parachute, and start to perform in situ measurements in the stratosphere to help characterize the location and properties of the tropopause, and continue into the troposphere to pressures of at least 10 bar. All of the science objectives, except for the abundance of oxygen which may be only addressed partially, can be achieved by reaching 10 bar. Previous studies have shown that depths beyond 10 bar become increasingly more difficult to achieve for several technology reasons; for example: (i) the descent time, hence the relay duration, would increase and make the relay geometry more challenging; (ii) the technology for the probe may change at pressures greater than 10 bar; (iii) the opacity of the atmosphere to radio-frequencies increases with depth and may make the communication link even more challenging at higher pressures. Future studies would be needed to conduct a careful assessment of the trade-offs between science return and the added complexity of a probe that could operate at pressures greater than 10 bar. Accelerometry measurements may also be performed during the entry phase in the higher part of the stratosphere to probe the upper layers of the atmosphere prior to starting in situ measurements under parachute.

A carrier spacecraft would be required to deliver the probe to the desired atmospheric entry point at Saturn. We have identified three possible mission configurations:

- Configuration 1: Probe + Carrier: The probe would detach from the carrier spacecraft prior to probe entry. The carrier would follow the probe path and be destroyed during atmospheric entry, but may be capable of performing pre-entry science. The carrier would not be used as a radio relay to transmit the probe data to Earth. The probe would transmit its data to the ground system via a direct-to-Earth (DTE) RF link.
- Configuration 2: Probe + Carrier/Relay: The probe would detach from the carrier several months prior to probe entry. Subsequent to probe release, the carrier trajectory would be deflected to prepare for over-flight phasing of the probe descent location for both probe data relay and performing approach and flyby science.

- *Configuration* 3: *Probe + Orbiter*: This configuration would be similar to the Galileo Orbiter/Probe mission. The probe would detach from the orbiter several months prior to probe entry. As for Configuration 2, subsequent to probe release, the orbiter trajectory would be deflected to prepare for over-flight phasing of the probe descent location. After probe relay during over-flight, the orbiter would be placed in orbit around Saturn and continue to perform orbital science.

Configuration 1 would allow the carrier to perform months of approach science and *in situ* pre-entry science. In this architecture, the probe data transmission would rely solely on a Direct-to-Earth probe telecommunications link. In addition to being used as the probe relay data following completion of the probe mission, Configuration 2 would possibly also provide the capability to perform months of approach science, but in addition flyby science (for a few days). This configuration would allow many retransmissions of the probe data for redundancy. Configuration 3 would clearly be the most capable, but most costly configuration. Trade-off studies will need to be carried out to assess whether the supporting remote sensing observations may be achievable during the approach phase and a single flyby or from an orbiter. Any of the carrier options could provide context observations but an orbiter could bring more science return in addition to supporting the probe science. The only requirement is that those data be downlinked to Earth while the spacecraft is still operating. For example, useful observations from a Configuration 1 carrier could be made several hours before probe entry, and downlink could be accomplished in the intervening time. Finally, it may be worth studying if the emerging solar-sail propulsion technology (Janhunen et al., 2014) can be considered for this option.

4.1. Atmospheric entry probe

An atmospheric entry probe at Saturn would in many respects resemble the Jupiter Galileo probe. The concept was put forward for Saturn in the KRONOS mission proposal (Marty et al., 2009). Giant Planet probe concept studies have been studied by ESA in 2010.[6] As an example, the KRONOS probe had a mass of ~337 kg, with a 220 kg deceleration module (aeroshell, thermal protection system, parachutes and separation hardware) and a 117 kg descent module, including the probe structure, science instruments, and subsystems. It is anticipated that the probe architecture for this mission would be battery powered and accommodate either a DTE link or a data relay to the carrier or the orbiter. Trades would be done to assess the complexity (and cost) of probe and telecomm link design as a function of operational depth in the atmosphere. A representative payload for the Saturn probe that would allow addressing the science objectives identified in Sections 2 and 3 is shown in Table 5.

4.2. Carrier or orbiter

Alternative architectures for the carrier (Configuration 1 or 2) or the orbiter (Configuration 3) would be considered, taking into account, if possible and if technologically and programmatically sound, the heritage for outer planet/deep space missions within either ESA or NASA. As an example, the carrier or the orbiter may benefit from subsystems developed by either ESA or NASA for previous outer planet missions (for example ESA/JUICE or NASA/JUNO, or possibly NASA/ESA Cassini–Huygens).

4.3. Power generation

It would be worth studying whether the proposed mission architectures could be solely designed on batteries and solar power. It would require qualification of the low-intensity low-temperature (LILT) solar cell arrays for 9.5 AU conditions. The probe would be powered with primary batteries as were the Galileo and Huygens probes. In all three configurations, the carrier (configuration 1 and 2) or the orbiter (configuration 3) would be equipped with a combination of solar panels, secondary batteries and possibly a set of primary batteries for phases that require a high power input, for example during the probe entry phase. Nuclear power would be considered for the carrier or the orbiter only if available solar power technology would be found to be unfeasible.

4.4. Interplanetary trajectory and entry zone of the probe

Many trajectory options have been identified, using both direct and gravity-assisted transfers to Saturn, and more will be identified in subsequent studies. Trajectory selection will be based on the selected carrier option, launch vehicle capabilities, and available probe thermal protection capability. The interplanetary trajectory and the probe entry location are inseparably linked. Saturn's extensive ring system presents a severe collision hazard to an inbound probe. For various declinations of the spacecraft's approach asymptote, some latitudes will be inaccessible because the trajectories to deliver those latitudes would impact the rings. Also, although it is possible to adjust the inclination of the approach orbit for the purposes of accessing a desired latitude, this approach can greatly increase the atmosphere-relative entry speeds, possibly driving the mission to an expensive heat shield material technology development. During the studies, the issues of probe entry locations, approach and entry trajectories, and probe technologies must be treated together. Due to Saturn's large obliquity and the characteristics of reasonable Earth-to-Saturn transfer trajectories, the best combinations change with time. Concerning the probe entry zone, both equatorial and mid-latitude regions may be a representative location from the scientific point of view (see a discussion in Section 3.3). Volatile-depleted regions are probably located at the cyclones in both poles and may also be located at the so-called "storm-alley" (region of low static stability able to develop updrafts and downdrafts). More generally, the peaks of westward jets can be unstable based on the stability of the wind system and eastward jets (particularly the anticyclonic branch of eastward jets) might be good locations to retrieve the deep values of volatiles at higher levels in the atmosphere (Read et al., 2009). In any case, there are several potential entry points and a decision where to enter, for example from the point of view of jets dynamics, is not evident, and will require further study. However, from cloud tracking, a significant vertical wind shear has been inferred in the equatorial eastward jet and less intense vertical wind shear in the rest of eastward jets (García-Melendo et al., 2010). On the other hand, westward jets seem to have no vertical wind shear at the levels that can be studied from cloud tracking with Cassini images (García-Melendo et al., 2009).

4.5. International collaboration

In this paper, we only consider ESA/Europe and NASA/USA collaborations but collaborations with other international partners may be envisaged. One of the key probe technologies for a Saturn probe that would be new for European industry is the heat shield material. Recent NASA studies concerning entry system performance requirements versus thermal protection system capability for a Saturn entry probe have been completed (Ellerby et al., 2013).

Table 5
Measurement requirements.

Instrument	Measurement
Mass spectrometer	Elemental and chemical composition
	Isotopic composition
	High molecular mass organics
Helium abundance detector	Accurate He/H_2 ratio
Atmospheric Structure Instrument	Pressure, temperature, density, molecular weight profile, lightning detector
Doppler Wind Experiment	Measure winds, speed and direction
Nephelometer	Cloud structure
	Solid/liquid particles
Net-flux radiometer	Thermal/solar energy

This example is used to illustrate that, should Europe be willing to lead the probe development (as was so successfully done with Huygens), careful consideration of trade-offs would have to be made for either development of this new technology within Europe or for establishing an international collaboration with NASA. International collaboration may also be considered for other mission elements, including the carrier (and of course the orbiter if configuration 3 would be further studied), navigation, the probe data relay, the ground segment, and science payload. All three configurations would be achievable through different schemes of collaboration between Europe and the USA. As an example, configurations 1 and 2 may take the form of a combined ESA/Class-M and a NASA Discovery or New Frontiers collaboration, if such a scheme were to become programmatically feasible as it is currently not the case. Configuration 3 would be achievable through a collaboration that would involve an ESA/Class M and a NASA/Flagship mission. We do not put forward an ESA/Class L mission at this stage as the current ESA Cosmic Vision plan would not allow a new Class-L mission before the late 30s/early 40s.

5. Characteristics of a possible probe model payload

The scientific requirements discussed above can be addressed with a suite of scientific instruments, which are given in Table 5 and discussed in the following. Note that this list of instruments should not be considered as a unique payload complement but as guideline for some of the instruments we might wish to see on board. For example, an alternative to both the nephelometer and net flux radiometer described below are elements of the Huygens Descent Imager/Spectral Radiometer (DISR) (Tomasko et al., 2002) that used the sun as a source. Ultimately, the payload of the Saturn probe would be the subject of detailed mass, power and design trades, but should seek to address the majority of the scientific goals outlined in Sections 2 and 3.

5.1. Mass spectrometry

The chemical and isotopic composition of Saturn's atmosphere, and its variability, will be measured by mass spectrometry. The gas analysis systems for a Saturn Probe may benefit from a high heritage from instrumentation already flown and having provided atmospheric composition and isotope investigations. The scientific objective for the mass spectrometric investigation regarding Saturn's formation and the origin of the solar system are *in situ* measurements of the chemical composition and isotope abundances in the atmosphere, such as H, C, N, S, P, Ge, As, noble gases He, Ne, Ar, Kr, and Xe, and the isotopes D/H, $^{13}C/^{12}C$, $^{15}N/^{14}N$, $^{3}He/^{4}He$, $^{20}Ne/^{22}Ne$, $^{38}Ar/^{36}Ar$, $^{36}Ar/^{40}Ar$, and those of Kr and Xe.

At Jupiter, the Galileo Probe Mass Spectrometer (GPMS) experiment (Niemann et al., 1992) was used, which was designed to measure the chemical and isotopic composition of Jupiter's atmosphere in the pressure range from 0.15 to 20 bar by *in situ* sampling of the ambient atmospheric gas. The GPMS consisted of a gas sampling system that was connected to a quadrupole mass spectrometer. The gas sampling system also had two sample enrichment cells, allowing for enrichments of hydrocarbons by a factor 100–500, and one noble gas analysis cell with an enrichment factor of about 10. Low abundance noble gases can be measured by using an enrichment cell, as used on the Galileo mission (Niemann et al., 1996). From GPMS measurements the Jupiter He/H_2 ratio was determined as 0.156 ± 0.006. To improve the accuracy of the measurement of the He/H_2 ratio and isotopic ratios by mass spectrometry the use of reference gases will be necessary. On the Rosetta mission the ROSINA experiment carries for each mass spectrometer a gas calibration unit (Balsiger et al., 2007). Similarly, the SAM experiment on the Curiosity rover can use either a gas sample from its on-board calibration cell or utilize one of the six individual metal calibration cups on the sample manipulation system (Mahaffy et al., 2012).

A major consideration for the mass spectrometric analysis is how to distinguish between different molecular species with the same nominal mass, *e.g.*, N_2 and CO, from the complex mixture of gases in Saturn's atmosphere. There are two approaches available, one is high resolution mass spectrometry with sufficient mass resolution to resolve the isobaric interferences, and the other is chemical pre-separation of the sample followed by low resolution mass spectrometry.

5.1.1. High resolution mass spectrometry

Probably the first composition experiment with high resolution mass spectrometry is the ROSINA experiment on the Rosetta mission (Balsiger et al., 2007) which has a Reflectron-Time-of-Flight (RTOF) instrument with a mass resolution of about $m/\Delta m = 5000$ at 50% peak height (Scherer et al., 2006), Double-Focussing Mass Spectrometer (DFMS) with a mass resolution of about $m/\Delta m = 9000$ at 50% peak height, and a pressure gauge. Determination of isotope ratios at the 1% accuracy level has been accomplished during the cruise phase. A time-of-flight instrument with even more mass resolution has been developed for possible application in Titan's atmosphere, which uses a multi-pass time-of-flight configuration (Waite et al., 2014). Typical mass resolutions are $m/\Delta m = 13,500$ at 50% peak height and 8500 at 20% peak height. In bunch mode the mass resolution can be increased to 59,000 (at 50% peak height). Again, determination of isotope ratios at the 1% accuracy level has been accomplished. An alternative multi-pass time-of-flight instrument has been developed by Okumura et al. (2004), which uses electric sectors instead of ion mirrors for time and space focussing. Mass resolutions up to $m/\Delta m = 350,000$ have been reported (Toyoda et al., 2003).

Recently, a new type of mass spectrometer, the Orbitrap mass spectrometer, was introduced (Makarov, 2000; Hu et al., 2005), which uses ion confinement in a harmonic electrostatic potential. The

Orbitrap mass spectrometer is a Fourier-Transform type mass spectrometer, and it allows for very high mass resolutions in a compact package. For example, using an Orbitrap mass spectrometer for laboratory studies of chemical processes in Titan's atmosphere, mass resolutions of $m/\Delta m = 100{,}000$ have been accomplished up to $m/z = 400$ (Hörst et al., 2012), and $m/\Delta m = 190{,}000$ at 50% peak height and $m/z = 56$ in a prototype instrument for the JUICE mission (Briois et al., 2013).

5.1.2. Low resolution mass spectrometry with chemical pre-processing

The alternative approach to high resolution mass spectrometry, which was used successfully on many missions so far, is to use a simpler low resolution mass spectrometer together with a chemical processing of the sample to separate or eliminate isobaric interferences. One established way is to use chromatographic columns with dedicated chemical specificity for a separation of chemical substances before mass spectrometric analysis. The Gas-Chromatograph Mass Spectrometer (GCMS) of the Huygens Probe is a good example of such an instrument (Niemann et al., 2002, 2005, 2010). The Huygens Probe GCMS has three chromatographic columns, one column for separation of CO and N_2 and other stable gases, the second column for separation of nitriles and other organics with up to three carbon atoms, and the third column for the separation of C_3 through C_8 saturated and unsaturated hydrocarbons and nitriles of up to C_4. The GCMS was also equipped with a chemical scrubber cell for noble gas analysis and a sample enrichment cell for selective measurement of high boiling point carbon containing constituents. A quadrupole mass spectrometer was used for mass analysis with a mass range from 2 to 141 amu, which is able to measure isotope ratios with an accuracy of 1%. Newer examples of GCMS instrumentation are the Ptolemy instrument on the Rosetta lander for the measurement of stable isotopes of key elements (Wright et al., 2007), which uses an ion trap mass spectrometer, the COSAC instrument also on the Rosetta lander for the characterization of surface and sub-surface samples (Goesmann et al., 2007), which uses a time-of-flight mass spectrometer, and the SAM experiment on the Curiosity rover (Mahaffy et al., 2012), which uses a classical quadrupole mass spectrometer.

5.1.3. Summary of mass spectrometry

So far in most missions the chemical pre-separation was the technique used to avoid isobaric interferences in the mass spectra, with the exception of the mass spectrometer experiment ROSINA on the Rosetta orbiter. Chemical pre-separation works well, but by choosing chromatographic columns with a certain chemical specificity one makes a pre-selection of the species to be investigated in detail. This possibly is a limitation when exploring an object where little is known. Also, gas chromatographic systems with several columns are rather complex systems, both to build and to operate (see the SAM instrument as a state-of-the art example of this technique, Mahaffy et al., 2012).

In recent years there has been a significant development of compact mass spectrometers that offer high mass resolution, as outlined above, and these developments are still ongoing. Thus, solving the problem of isobaric interferences in the mass spectra by mass resolution can be addressed by mass spectrometry alone and one should seriously consider using high resolution mass spectrometry for a future mission to probe Saturn's atmosphere. After all, no *a priori* knowledge of the chemical composition has to be assumed. In addition, with modern time-of-flight mass spectrometers mass ranges beyond 1000 amu are not a problem at all, which would have been useful to investigate Titan's atmosphere. Nevertheless, some chemical pre-selection may still be considered even for high resolution mass spectrometry. For example, the cryotrapping technique, which has a long history in the laboratory, would enable detection of noble gases at abundances as low as 0.02 ppb (Waite et al., 2014).

5.1.4. Tunable laser system

A Tunable Laser Spectrometer (TLS) (Durry et al., 2002) can be employed as part of a GC system to measure the isotopic ratios to a high accuracy of specific molecules, *e.g.* H_2O, NH_3, CH_4, CO_2 and others. TLS employs ultra-high spectral resolution (0.0005 cm^{-1}) tunable laser absorption spectroscopy in the near infra-red (IR) to mid-IR spectral region. TLS is a direct non-invasive, simple technique that for small mass and volume can produce remarkable sensitivities at the sub-ppb level for gas detection. Species abundances can be measured with accuracies of a few %, and isotope determinations are with about 0.1% accuracy. With a TLS system one can derive the isotopic ratios of D/H, $^{18}O/^{16}O$, $^{13}C/^{12}C$, $^{18}O/^{16}O$, and $^{17}O/^{16}O$.

For example, TLS was developed for application in the Mars atmosphere (Le Barbu et al., 2004), within the ExoMars mission; a recent implementation of a TLS system was for the Phobos Grunt mission (Durry et al., 2010), and is on the SAM instrument (Webster and Mahaffy, 2011), which was used to measure the isotopic ratios of D/H and of $^{18}O/^{16}O$ in water and $^{13}C/^{12}C$, $^{18}O/^{16}O$, $^{17}O/^{16}O$, and $^{13}C^{18}O/^{12}C^{16}O$ in carbon dioxide in the Martian atmosphere (Webster et al., 2013).

5.2. Helium Abundance Detector

The Helium Abundance Detector (HAD), as it was used on the Galileo mission (von Zahn and Hunten, 1992), basically measures the refractive index of the atmosphere in the pressure range of 2–10 bar. The refractive index is a function of the composition of the sampled gas, and since the jovian atmosphere consists of mostly of H_2 and He, to more than 99.5%, the refractive index is a direct measure of the He/H_2 ratio. The refractive index can be measured by any two-beam interferometer, where one beam passes through a reference gas and the other beam through atmospheric gas. The difference in the optical path gives the difference in refractive index between the reference and atmospheric gas. For the Galileo mission a Jamin–Mascart interferometer was used, because of its simple and compact design, with an expected accuracy of the He/H_2 ratio of ± 0.0015. The accomplished measurement of the He mole fraction gave 0.1350 ± 0.0027 (von Zahn et al., 1998), with a somewhat lower accuracy when expected, but still better than is possible by a mass spectrometric measurement.

5.3. Atmospheric Structure Instrument

The key *in situ* measurements by an Atmospheric Structure Instrument (ASI) would be the accelerometry during the probe entry phase and pressure, temperature and mean molecular weight during descent. The atmospheric density is derived from these measurements. There is strong heritage from the Huygens ASI experiment (HASI) of the Cassini–Huygens mission (Fulchignoni et al., 2002). Furthermore, these types of sensors have been selected for NASA's Mars Science Laboratory (MSL) and are part of the meteorological package of ESA's Exomars mission. *In situ* atmospheric structure measurements are essential for the investigation of the planet's atmospheric structure and dynamics. The estimation of the temperature lapse rate can be used to identify the presence of condensation and possible clouds, to distinguish between saturated and unsaturated, stable and conditionally stable regions. The variations in the density, pressure and temperature profiles provide information on the atmospheric stability and stratification, on the presence of winds, thermal tides, waves and turbulence in the

atmosphere. A typical Atmospheric Structure Instrument would consist of three primary sensor packages: a three-axis accelerometer, a pressure profile instrument and temperature sensors. It would start to operate right at the beginning of the entry phase of the probe, sensing the atmospheric drag experienced during entry. Direct pressure and temperature measurement could be performed by the sensors having access to the atmospheric flow from the earliest portion of the descent until the end of the probe mission at approximately 10 bar.

ASI data will also contribute to the analysis of the atmospheric composition, since it will monitor the acceleration experienced by the probe during the whole descent phase. ASI will provide the unique direct measurements of pressure and temperature through sensors having access to the atmospheric flow.

5.3.1. Accelerometers

The accelerator package, a 3-axis accelerometer, should be placed as close as possible to the center of mass of the entry probe. Like on Huygens, the main sensor could be a highly sensitive servo-accelerometer aligned along the vertical axis of the Probe, with a resolution of $1–10 \times 10^{-5} \, \mathrm{m \, s^{-2}}$ with an accuracy of 1%. Probe acceleration can be measured in the range of 0–2000 $\mathrm{m \, s^{-2}}$ (Zarnecki et al., 2004). Assuming the HASI accelerometer performance at Titan, a noise level of about $3 \times 10^{-8} \, \mathrm{m \, s^{-2}}$ is expected. The exact performance achievable, in terms of the accuracy of the derived atmospheric density, will also depend on the probe ballistic coefficients, entry speed and drag coefficient.

5.3.2. Temperature sensors

As in the Huygens Probe, the temperature sensors will use platinum resistance thermometers. These are exposed to the atmospheric flow and are effectively thermally isolated from the support structure. The principle of measurement is based on the variation of the resistance of the metallic wire with temperature. TEM has been designed to have a good thermal coupling between the sensor and the atmosphere and to achieve high accuracy and resolution. Over the temperature range of 60–330 K these sensors maintain an accuracy of 0.1 K with a resolution of 0.02 K.

5.3.3. Pressure Profile Instrument

The Pressure Profile Instrument (PTI) will measure the pressure during the entire descent with an accuracy of 1% and a resolution of 10^{-6} bar. The atmospheric flow is conveyed through a Kiel probe inside the probe where the transducers and related electronic are located. The transducers are silicon capacitive sensors with pressure dependant dielectricum. The pressure sensor contains as dielectricum a small vacuum chamber between the two electrode plates, with the external pressure defining the distance of these plates. Detectors with diaphragms of different pressure sensitivities will be utilized to cover the pressure range to ∼10 bar. The pressure is derived as a frequency measurement (within 3–20 kHz range) and the measurements internally compensate for thermal and radiation influences.

5.3.4. Atmospheric Electricity Package

Similar to HASI on the Huygens Probe, a lightning detector can perform passive electric or magnetic field measurements in two different frequency ranges. For HASI, the analog electric field signals were amplified, digitized, sampled, windowed, and Fourier-transformed onboard to obtain electric field spectra in the frequency ranges of 0–11.5 kHz and 3–96 Hz. On Earth, lightning radio emissions in the VLF band (3–30 kHz) can propagate over several thousands of kilometers due to ionospheric reflections. This should work as well at Saturn, and the strength of Saturn lightning, which is expected to be superbolt-like (Dyudina et al., 2013), should enable an easy detection in case a thunderstorm is present. It might be more difficult to detect the weak Schumann resonances, where the lowest eigenfrequency for Saturn is expected to occur around 0.7–0.8 Hz (Simões et al., 2012). For conductivity measurements of the atmosphere a mutual impedance probe or a relaxation probe can carry out active electric field measurements.

5.4. Doppler Wind Experiment

The primary goal of a Doppler Wind Experiment (DWE) on a Saturn probe would be to measure a vertical profile of the zonal (east–west) winds along the probe descent path. A secondary goal of the DWE is to detect, characterize, and quantify microstructure in the probe descent dynamics, including probe spin, swing, aerodynamic buffeting and atmospheric turbulence, and to detect regions of wind shear and atmospheric wave phenomena. Because of the need for accurate probe and carrier trajectories for making the Doppler wind measurement, the DWE must be closely coordinated with the navigation and radiometric tracking of the carrier, and the probe entry and descent trajectory reconstructions. A Doppler Wind Experiment could be designed to work with a probe DTE communication architecture or a probe-to-relay architecture. Both options include ultra-stable oscillator (USO) requirements and differ only in the angle of entry and DTE geometry requirements. For relay, the system comprises a probe and a carrier USO as part of the probe–carrier communication package. The experiment would benefit from the heritage of both the Galileo and Huygens Doppler Wind Experiments (Atkinson et al., 1998; Bird et al., 2002).

5.5. Nephelometer

The composition and precise location of cloud layers in Saturn are largely unknown. They may be composed of ammonia, ammonium hydrosulfide, or simply water. Because of this relative paucity of information on Saturn's clouds, the demands we place on a cloud particle sensor, a nephelometer, are significant. Such an instrument would have little heritage in planetary exploration, beyond the one on the Galileo probe. There are similar laser driven, fiber fed nephelometers used in very similar settings on Earth (e.g., Barkey and Liou, 2001; Barkey et al., 1999; Gayet et al., 1997). However, these were shrouded designs, which is mass-prohibitive on a planetary probe, and they also did not attempt to measure the polarization ratio phase function, because they knew their aerosols were water. The polarization modulation technique that we are proposing was first described by Hunt and Huffman (1973), and has been used in laboratory settings by several groups (e.g., Kuik et al., 1991). While the precise implementation of the instrument is novel to planetary science, and the polarization modulation technique is also new to an in situ instrument, the technology needed to carry out this instrument is all relatively modest. This nephelometer would measure not only the amplitude phase function of the light scattered by the clouds from a laser source on the probe, but also the polarization ratio phase function as well.

5.6. Net Energy Flux Radiometer

A Net Energy Flux Radiometer (NFR) measures the thermal profile and heat budget in the atmosphere. Such a NFR instrument was part of the scientific payload of the Galileo mission (Sromovsky et al., 1992), which measured the vertical profile of upward and downward radiation fluxes in the region between 0.44 and 14 bar region (Sromovsky et al., 1998). Radiation was measured in five wavelength bands, 0.3–3.5 μm (total solar radiation), 0.6–3.5 μm (total solar radiation in methane absorption region), 3–500 μm (deposition and loss of thermal radiation), 3.5–5.8 μm (water vapor and cloud structure), and 14–35 μm (water vapor). On Galileo, NFR

found signatures of NH$_3$ ice clouds and NH$_4$SH clouds (Sromovsky et al., 1998), however, water fraction was found to be much lower than solar and no water clouds could be identified.

6. Conclusions

In this paper, we have shown that the *in situ* exploration of Saturn can address two major science themes: the formation history of our solar system and the processes at work in the atmospheres of giant planets. We provided a list of recommended measurements in Saturn's atmosphere that would allow disentangling between the existing giant planets formation scenarios and the different volatile reservoirs from which the solar system bodies were assembled. Moreover, we illustrated how an entry probe would reveal new insights concerning the vertical structures of temperatures, density, chemical composition and clouds during atmospheric descent. In this context, the top level science goals of a Saturn probe mission would be the determination of:

1. the atmospheric temperature, pressure and mean molecular weight profiles;
2. the abundances of cosmogenically abundant species C, N, S and O;
3. the abundances of chemically inert noble gases He, Ne, Xe, Kr and Ar;
4. the isotopic ratios in hydrogen, oxygen, carbon, nitrogen, He, Ne, Xe, Kr and Ar;
5. the abundances of minor species delivered by vertical mixing (*e.g.*, P, As, Ge) from the deeper troposphere, photochemical species (*e.g.*, hydrocarbons, HCN, hydrazine and diphosphine) in the troposphere and exogenic inputs (oxygenated species) in the upper atmosphere;
6. the particle optical properties, size distributions, number and mass densities, opacity, shapes and composition.

Additional *in situ* science measurements aiming at investigating the global electric circuit on Saturn could also be considered (measurement of the Schumann resonances, determination of the vertical profile of conductivity and the spectral power of Saturn lightning at frequencies below the ionospheric cutoff, etc.).

We advocated that a Saturn mission incorporating elements of *in situ* exploration should form an essential element of ESA and NASA's future cornerstone missions. We described the concept of a Saturn probe as the next natural step beyond Galileo's *in situ* exploration of Jupiter, and the Cassini spacecraft's orbital reconnaissance of Saturn. Several mission designs have been discussed, all including a spacecraft carrier/orbiter and a probe that would derive from the KRONOS concept previously proposed to ESA (Marty et al., 2009). International collaborations, in particular between NASA/USA and ESA/Europe may be envisaged in the future to enable the success of a mission devoted to the *in situ* exploration of Saturn.

References

Alibert, Y., Mousis, O., Benz, W., 2005a. On the volatile enrichments and composition of Jupiter. Astrophys. J. 622, L145–L148.

Alibert, Y., Mousis, O., Mordasini, C., Benz, W., 2005b. New Jupiter and Saturn formation models meet observations. Astrophys. J. 626, L57–L60.

Asplund, M., Grevesse, N., Sauval, A.J., Scott, P., 2009. The chemical composition of the Sun. Annu. Rev. Astron. Astrophys. 47, 481–522.

Atkinson, D.H., Pollack, J.B., Seiff, A., 1998. The Galileo probe Doppler wind experiment: measurement of the deep zonal winds on Jupiter. J. Geophys. Res. 103, 22911–22928.

Atreya, S.K., Mahaffy, P.R., Niemann, H.B., Wong, M.H., Owen, T.C., 2003. Composition and origin of the atmosphere of Jupiter—an update, and implications for the extrasolar giant planets. Planet. Space Sci. 51, 105–112.

Atreya, S.K., Wong, M.H., Owen, T.C., Mahaffy, P.R., Niemann, H.B., de Pater, I., Drossart, P., Encrenaz, T., 1999. A comparison of the atmospheres of Jupiter and Saturn: deep atmospheric composition, cloud structure, vertical mixing, and origin. Planet. Space Sci. 47, 1243–1262.

Baines, K.H., Carlson, R.W., Kamp, L.W., 2002. Fresh ammonia ice clouds in Jupiter. I. Spectroscopic identification, spatial distribution, and dynamical implications. Icarus 159, 74–94.

Baldwin, M.P., et al., 2001. The quasi-biennial oscillation. Rev. Geophys. 39, 179–229.

Balsiger, H., et al., 2007. Rosina—Rosetta Orbiter Spectrometer for Ion and Neutral Analysis. Space Science Rev. 128, 745–801.

Barkey, B., Liou, K.N., Gellerman, W., Sokolsky, P., 1999. An analog light scattering experiment of hexagonal icelike particles. I. Experimental apparatus and test measurements. J. Atmos. Sci. 56 (4), 605–612.

Barkey, B., Liou, K.N., 2001. Polar nephelometer for light-scattering measurements of ice crystals. Opt. Lett. 26 (4), 232–234.

Bézard, B., Greathouse, T., Lacy, J., Richter, M., Griffith, C.A., 2003. The D/H ratio in Jupiter and Saturn from high-resolution spectral observations near 8.6 µm. Bull. Am. Astron. Soc. 35, 1017.

Bézard, B., Lellouch, E., Strobel, D., Maillard, J.-P., Drossart, P., 2002. Carbon monoxide on Jupiter: evidence for both internal and external sources. Icarus 159, 95–111.

Bird, M.K., et al., 2002. The Huygens Doppler wind experiment—titan winds derived from probe radio frequency measurements. Space Science Rev. 104, 613–640.

Boss, A.P., 2001. Formation of planetary-mass objects by protostellar collapse and fragmentation. Astrophys. J. 551, L167–L170.

Boss, A.P., 1997. Giant planet formation by gravitational instability. Science 276, 1836–1839.

Briggs, F.H., Sackett, P.D., 1989. Radio observations of Saturn as a probe of its atmosphere and cloud structure. Icarus 80, 77–103.

Briois, C., et al., 2013. Dust orbitrap sensor (DOTS) for in-situ analysis of airless planetary bodies. In: Lunar and Planetary Institute Science Conference Abstracts 44, p. 2888.

Cavalié, T., Moreno, R., Lellouch, E., Hartogh, P., Venot, O., Orton, G.S., Jarchow, C., Encrenaz, T., Selsis, F., Hersant, F., Fletcher, L.N., 2014. The first submillimeter observation of CO in the stratosphere of Uranus. Astronomy and Astrophysics 562, A33.

Cavalié, T., Hartogh, P., Billebaud, F., Dobrijevic, M., Fouchet, T., Lellouch, E., Encrenaz, T., Brillet, J., Moriarty-Schieven, G.H., 2010. A cometary origin for CO in the stratosphere of Saturn? Astron. Astrophys. 510, A88.

Cavalié, T., Billebaud, F., Dobrijevic, M., Fouchet, T., Lellouch, E., Encrenaz, T., Brillet, J., Moriarty-Schieven, G.H., Wouterloot, J.G.A., Hartogh, P., 2009. First observation of CO at 345 GHz in the atmosphere of Saturn with the JCMT: new constraints on its origin. Icarus 203, 531–540.

Chambers, J.E., Wetherill, G.W., 2001. Planets in the asteroid belt. Meteorit. Planet. Sci. 36, 381–399.

Conrath, B.J., Gautier, D., 2000. Saturn Helium abundance: a reanalysis of voyager measurements. Icarus 144, 124–134.

de Graauw, T., et al., 1997. First results of ISO-SWS observations of Saturn: detection of CO$_2$, CH$_3$C$_2$H, C$_4$H$_2$ and tropospheric H$_2$O. Astron. Astrophys. 321, L13–L16.

Del Genio, A.D., Achterberg, R.K., Baines, K.H., Flasar, F.M., Read, P.L., Sánchez-Lavega, A., Showman, A.P., 2009. Saturn atmospheric structure and dynamics. In: Saturn from Cassini–Huygens, p. 113.

Dodson-Robinson, S.E., Bodenheimer, P., 2010. The formation of Uranus and Neptune in solid-rich feeding zones: connecting chemistry and dynamics. Icarus 207, 491–498.

Durry, G., et al., 2010. Near infrared diode laser spectroscopy of C$_2$H$_2$, H$_2$O, CO$_2$ and their isotopologues and the application to TDLAS, a tunable diode laser spectrometer for the martian PHOBOS-GRUNT space mission. Appl. Phys. B: Lasers Opt. 99, 339–351.

Durry, G., Hauchecorne, A., Ovarlez, J., Ovarlez, H., Pouchet, I., Zeninari, V., Parvitte, B., 2002. In situ measurement of H$_2$O and CH$_4$ with telecommunication laser diodes in the lower stratosphere: dehydration and indication of a tropical air intrusion at mid-latitudes. J. Atmos. Chem. 43 (3), 175–194.

Dyudina, U.A., Ingersoll, A.P., Ewald, S.P., Porco, C.C., Fischer, G., Yair, Y., 2013. Saturn's visible lightning, its radio emissions, and the structure of the 2009–2011 lightning storms. Icarus 226, 1020–1037.

Dyudina, U.A., Ingersoll, A.P., Ewald, S.P., Porco, C.C., Fischer, G., Kurth, W.S., West, R. A., 2010. Detection of visible lightning on Saturn. Geophys. Res. Lett. 37, 9205.

Ellerby, D., Venkatapathy, E., Stackpoole, M., Chinnapongse, R., Beerman, A., Feldman, J., Peterson, K., Prahbu, D., Munk, M., 2013. Woven thermal protection system (WTPS) a novel approach to meet NASA's most demanding reentry missions. In: 10th International Planetary Probe Workshop, Session 8B: Cross Cutting Technologies III.

Fegley Jr., B., Lodders, K., 1994. Chemical models of the deep atmospheres of Jupiter and Saturn. Icarus 110, 117–154.

Fegley Jr., B., Prinn, R.G., 1985. Equilibrium and nonequilibrium chemistry of Saturn's atmosphere—implications for the observability of PH3, N2, CO, and GeH4. Astrophys. J. 299, 1067–1078.

Fischer, G., Gurnett, D.A., Kurth, W.S., Akalin, F., Zarka, P., Dyudina, U.A., Farrell, W.M., Kaiser, M.L., 2008. Atmospheric electricity at Saturn. Space Sci. Rev. 137, 271–285.

Fletcher, L.N., et al., 2012. Sub-millimetre spectroscopy of Saturn's trace gases from Herschel/SPIRE. Astron. Astrophys. 539, A44.

Fletcher, L.N., Baines, K.H., Momary, T.W., Showman, A.P., Irwin, P.G.J., Orton, G.S., Roos-Serote, M., Merlet, C., 2011. Saturn's tropospheric composition and clouds from Cassini/VIMS 4.6–5.1 μm nightside spectroscopy. Icarus 214, 510–533.

Fletcher, L.N., Orton, G.S., Teanby, N.A., Irwin, P.G.J., 2009a. Phosphine on Jupiter and Saturn from Cassini/CIRS. Icarus 202, 543–564.

Fletcher, L.N., Orton, G.S., Teanby, N.A., Irwin, P.G.J., Bjoraker, G.L., 2009b. Methane and its isotopologues on Saturn from Cassini/CIRS observations. Icarus 199, 351–367.

Feuchtgruber, H., Lellouch, E., de Graauw, T., Bézard, B., Encrenaz, T., Griffin, M., 1997. External supply of oxygen to the atmospheres of the giant planets. Nature 389, 159–162.

Folkner, W.M., Woo, R., Nandi, S., 1998. Ammonia abundance in Jupiter's atmosphere derived from the attenuation of the Galileo probe's radio signal. J. Geophys. Res. 103, 22847–22856.

Fortney, J.J., Nettelmann, N., 2010. The interior structure, composition, and evolution of giant planets. Space Sci. Rev. 152, 423–447.

Fortney, J.J., Hubbard, W.B., 2003. Phase separation in giant planets: inhomogeneous evolution of Saturn. Icarus 164, 228–243.

Fouchet, T., Moses, J.I., Conrath, B.J., 2009. Saturn: composition and chemistry. In: Saturn from Cassini–Huygens, p. 83.

Fouchet, T., Guerlet, S., Strobel, D.F., Simon-Miller, A.A., Bézard, B., Flasar, F.M., 2008. An equatorial oscillation in Saturn's middle atmosphere. Nature 453, 200–202.

Fouchet, T., Irwin, P.G.J., Parrish, P., Calcutt, S.B., Taylor, F.W., Nixon, C.A., Owen, T., 2004. Search for spatial variation in the jovian $^{15}N/^{14}N$ ratio from Cassini/CIRS observations. Icarus 172, 50–58.

Fouchet, T., Lellouch, E., Bézard, B., Encrenaz, T., Drossart, P., Feuchtgruber, H., de Graauw, T., 2000. ISO-SWS observations of Jupiter: measurement of the ammonia tropospheric profile and of the $^{15}N/^{14}N$ isotopic ratio. Icarus 143, 223–243.

Friedson, A.J., 1999. New observations and modelling of a QBO-like oscillation in Jupiter's stratosphere. Icarus 137, 34–55.

Fulchignoni, M., et al., 2002. The characterisation of Titan's atmospheric physical properties by the Huygens atmospheric structure instrument (HASI). Space Sci. Rev. 104 (1), 397–434.

García-Melendo, E., Pérez-Hoyos, S., Sánchez-Lavega, A., Hueso, R., 2011. Saturn's zonal wind profile in 2004–2009 from Cassini ISS images and its long-term variability. Icarus 215, 62–74.

García-Melendo, E., Sánchez-Lavega, A., Legarreta, J., Perez-Hoyos, S., Hueso, R., 2010. A strong high altitude narrow jet detected at Saturn's equator. Geophys. Res. Lett. 37, 22204.

García-Melendo, E., Sánchez-Lavega, A., Rojas, J.F., Pérez-Hoyos, S., Hueso, R., 2009. Vertical shears in Saturn's eastward jets at cloud level. Icarus 201, 818–820.

Gautier, D., Hersant, F., 2005. Formation and composition of planetesimals. Space Sci. Rev. 116, 25–52.

Gautier, D., Hersant, F., Mousis, O., Lunine, J.I., 2001. Enrichments in volatiles in Jupiter: a new interpretation of the Galileo measurements. Astrophys. J. 550, L227–L230.

Gayet, J.F., Crépel, O., Fournol, J.F., Oshchepkov, S., 1997. A new airborne polar Nephelometer for the measurements of optical and microphysical cloud properties. Part I: theoretical design. Ann. Geophys. 15 (4), 451–459.

Goesmann, F., Rosenbauer, H., Roll, R., Szopa, C., Raulin, F., Sternberg, R., Israel, G., Meierhenrich, U., Thiemann, W., Munoz-Caro, G., 2007. Cosac, The Cometary Sampling and Composition experiment on Philae. Space Sci. Rev. 128, 257–280.

Gomes, R., Levison, H.F., Tsiganis, K., Morbidelli, A., 2005. Origin of the cataclysmic Late Heavy Bombardment period of the terrestrial planets. Nature 435, 466–469.

Guerlet, S., Fouchet, T., Bézard, B., Flasar, F.M., Simon-Miller, A.A., 2011. Evolution of the equatorial oscillation in Saturn's stratosphere between 2005 and 2010 from Cassini/CIRS limb data analysis. Geophys. Res. Lett. 38, s9201.

Guillot, T., Hueso, R., 2006. The composition of Jupiter: sign of a (relatively) late formation in a chemically evolved protosolar disc. Mon. Not. R. Astron. Soc. 367, L47–L51.

Guillot, T., 2004. Probing the giant planets. Phys. Today 57 040000-70.

Guillot, T., 1999. A comparison of the interiors of Jupiter and Saturn. Planet. Space Sci. 47, 1183–1200.

Hartogh, P., et al., 2011. Direct detection of the Enceladus water torus with Herschel. Astron. Astrophys. 532, L2.

Helled, R., Bodenheimer, P., 2014. The formation of Uranus and Neptune: challenges and implications for intermediate-mass exoplanets. Astrophys. J. 789, 69.

Helled, R., Guillot, T., 2013. Interior models of Saturn: including the uncertainties in shape and rotation. Astrophys. J. 767, 113.

Hersant, F., Gautier, D., Tobie, G., Lunine, J.I., 2008. Interpretation of the carbon abundance in Saturn measured by Cassini. Planet. Space Sci. 56, 1103–1111.

Hersant, F., Gautier, D., Lunine, J.I., 2004. Enrichment in volatiles in the giant planets of the Solar System. Planet. Space Sci. 52, 623–641.

Hickey, M.P., Walterscheid, R.L., Schubert, G., 2000. Gravity wave heating and cooling in Jupiter's thermosphere. Icarus 148, 266–281.

Hörst, S.M., et al., 2012. Formation of amino acids and nucleotide bases in a Titan atmosphere simulation experiment. Astrobiology 12, 809–817.

Hu, Q., Noll, R.J., Li, H., Makarov, A., Hardman, M., Cooks, R.G., 2005. The orbitrap: a new mass spectrometer. J. Mass Spectrom. 40 (4), 430–443.

Hunt, A.J., Huffman, D.R., 1973. The clouds of Venus—an experimental multiple scattering study of the polarization. Bull. Am. Astron. Soc. 5, 416.

Ida, S., Lin, D.N.C., 2004. Toward a deterministic model of planetary formation. I. A desert in the mass and semimajor axis distributions of extrasolar planets. Astrophys. J. 604, 388–413.

Janhunen, P., Lebreton, J.-P., Merikallio, S., Paton, M., Mengali, G., Quarta, A. 2014. Fast E-sail Uranus entry probe mission. Planet. Space. Sci, in press, http://dx.doi.org/10.1016/j.pss.2014.08.0044.

Johnson, T.V., Mousis, O., Lunine, J.I., Madhusudhan, N., 2012. Planetesimal compositions in exoplanet systems. Astrophys. J. 757, 192.

Kouchi, A., Yamamoto, T., Kozasa, T., Kuroda, T., Greenberg, J.M., 1994. Conditions for condensation and preservation of amorphous ice and crystallinity of astrophysical ices. Astron. Astrophys. 290, 1009–1018.

Kuik, F., Stammes, P., Streekstra, M.L., Hovenier, J.W., 1991. Measurements of scattering matrices of water droplets and ice crystals. In: Digest of the ICO Topical Meeting on Atmospheric, Volume and Surface Scattering, and Propagation, Florence, pp. 397–401.

Laraia, A.L., Ingersoll, A.P., Janssen, M.A., Gulkis, S., Oyafuso, F., Allison, M., 2013. Analysis of Saturn's thermal emission at 2.2-cm wavelength: spatial distribution of ammonia vapor. Icarus 226, 641–654.

Le Barbu, T., Vinogradov, I., Durry, G., Korablev, O., Chassefière, E., Bertaux, J.-L., 2004. Tdlas, a diode laser sensor for the in situ monitoring of H_2O and CO_2 isotopes. In: 35th COSPAR Scientific Assembly 35, p. 2115.

Leconte, J., Chabrier, G., 2013. Layered convection as the origin of Saturn's luminosity anomaly. Nat. Geosci. 6, 347–350.

Leconte, J., Chabrier, G., 2012. A new vision of giant planet interiors: impact of double diffusive convection. Astron. Astrophys. 540, A20.

Lellouch, E., Bézard, B., Fouchet, T., Feuchtgruber, H., Encrenaz, T., de Graauw, T., 2001. The deuterium abundance in Jupiter and Saturn from ISO-SWS observations. Astron. Astrophys. 370, 610–622.

Lewis, J.S., Prinn, R.G., 1980. Kinetic inhibition of CO and N_2 reduction in the solar nebula. Astrophys. J. 238, 357–364.

Lin, D.N.C., Papaloizou, J., 1986. On the tidal interaction between protoplanets and the protoplanetary disk. III—orbital migration of protoplanets. Astrophys. J. 309, 846–857.

Lodders, K., Palme, H., Gail, H.-P., 2009. Abundances of the elements in the solar system. In: Landolt Börnstein, p. 44.

Lodders, K., 2004. Jupiter formed with more tar than ice. Astrophys. J. 611, 587–597.

Magalhães, J.A., Seiff, A., Young, R.E., 2002. The stratification of Jupiter's troposphere at the Galileo probe entry site. Icarus 158, 410–433.

Mahaffy, P.R., et al., 2012. The sample analysis at Mars investigation and instrument suite. Space Sci. Rev. 170, 401–478.

Mahaffy, P.R., Niemann, H.B., Alpert, A., Atreya, S.K., Demick, J., Donahue, T.M., Harpold, D.N., Owen, T.C., 2000. Noble gas abundance and isotope ratios in the atmosphere of Jupiter from the Galileo probe mass spectrometer. J. Geophys. Res. 105, 15061–15072.

Makarov, A., 2000. Electrostatic axially harmonic orbital trapping: a high-performance technique of mass analysis. Anal. Chem. 72, 1156–1162.

Mandt, K.E., Waite, J.H., Lewis, W., Magee, B., Bell, J., Lunine, J., Mousis, O., Cordier, D., 2009. Isotopic evolution of the major constituents of Titan's atmosphere based on Cassini data. Planet. Space Sci. 57, 1917–1930.

Marley, M.S., Ackerman, A.S., Cuzzi, J.N., Kitzmann, D., 2013. Clouds and Hazes in Exoplanet Atmospheres. ArXiv e-prints arxiv:1301.5627.

Marty, B., Chaussidon, M., Wiens, R.C., Jurewicz, A.J.G., Burnett, D.S., 2011. A ^{15}N-poor isotopic composition for the solar system as shown by genesis solar wind samples. Science 332, 1533.

Marty, B., et al., 2009. Kronos: exploring the depths of Saturn with probes and remote sensing through an international mission. Exp. Astron. 23, 947–976.

McKeegan, Kevin, D., et al., 2006. Isotopic compositions of cometary matter returned by stardust. Science 314, 1724.

Miller, T.A., Wooldridge, M.S., Bozzelli, J.W., 2004. Computational modeling of the SiH_3+O_2 reaction and silane combustion. Combust. Flame 137, 73–92.

Mizuno, H., 1980. Formation of the giant planets. Prog. Theor. Phys. 64, 544–557.

Mordasini, C., Alibert, Y., Klahr, H., Henning, T., 2012. Characterization of exoplanets from their formation. I. Models of combined planet formation and evolution. Astron. Astrophys. 547, A111.

Moses, J.I., Fouchet, T., Bézard, B., Gladstone, G.R., Lellouch, E., Feuchtgruber, H., 2005. Photochemistry and diffusion in Jupiter's stratosphere: constraints from ISO observations and comparisons with other giant planets. J. Geophys. Res. (Planets) 110, 8001.

Mousis, O., Lunine, J.I., Madhusudhan, N., Johnson, T.V., 2012. Nebular water depletion as the cause of Jupiter's low oxygen abundance. Astrophys. J. 751, L7.

Mousis, O., Marboeuf, U., Lunine, J.I., Alibert, Y., Fletcher, L.N., Orton, G.S., Pauzat, F., Ellinger, Y., 2009. Determination of the minimum masses of heavy elements in the envelopes of Jupiter and Saturn. Astrophys. J. 696, 1348–1354.

Mousis, O., Alibert, Y., Benz, W., 2006. Saturn's internal structure and carbon enrichment. Astron. Astrophys. 449, 411–415.

Mousis, O., Gautier, D., Bockelée-Morvan, D., 2002. An evolutionary turbulent model of Saturn's subnebula: implications for the origin of the atmosphere of titan. Icarus 156, 162–175.

Nagy, A.F., Kliore, A.J., Mendillo, M., Miller, S., Moore, L., Moses, J.I., Müller-Wodarg, I., Shemansky, D., 2009. Upper atmosphere and ionosphere of Saturn. In: Saturn from Cassini–Huygens, p. 181.

Nettelmann, N., Püstow, R., Redmer, R., 2013. Saturn layered structure and homogeneous evolution models with different EOSs. Icarus 225, 548–557.

Niemann, H.B., Atreya, S.K., Demick, J.E., Gautier, D., Haberman, J.A., Harpold, D.N., Kasprzak, W.T., Lunine, J.I., Owen, T.C., Raulin, F., 2010. Composition of Titan's lower atmosphere and simple surface volatiles as measured by the Cassini–Huygens probe gas chromatograph mass spectrometer experiment. J. Geophys. Res. (Planets) 115, 12006.

Niemann, H.B., et al., 2005. The abundances of constituents of Titan's atmosphere from the GCMS instrument on the Huygens probe. Nature 438, 779–784.

Niemann, H.B., et al., 2002. The gas chromatograph mass spectrometer for the huygens probe. Space Sci. Rev. 104, 551–590.

Niemann, H.B., et al., 1998. The composition of the Jovian atmosphere as determined by the Galileo probe mass spectrometer. J. Geophys. Res. 103, 22831–22846.

Niemann, H.B., et al., 1996. The Galileo probe mass spectrometer: composition of Jupiter's atmosphere. Science 272, 846–849.

Niemann, H.B., Harpold, D.N., Atreya, S.K., Carignan, G.R., Hunten, D.M., Owen, T.C., 1992. Galileo probe mass spectrometer experiment. Space Sci. Rev. 60, 111–142.

Noll, K.S., Geballe, T.R., Knacke, R.F., 1995. Detection of H2 ^{18}O in Jupiter. Astrophys. J. 453, L49.

Okumura, D., Toyoda, M., Ishihara, M., Katakuse, I., 2004. A compact sector-type multi-turn time-of-flight mass spectrometer 'MULTUM II'. Nucl. Instrum. Methods Phys. Res. A 519, 331–337.

Orton, G.S., et al., 2008. Semi-annual oscillations in Saturn's low-latitude stratospheric temperatures. Nature 453, 196–199.

Orton, G.S., et al., 1998. Characteristics of the Galileo probe entry site from Earth-based remote sensing observations. J. Geophys. Res. 103, 22791–22814.

Owen, T., Mahaffy, P.R., Niemann, H.B., Atreya, S., Wong, M., 2001. Protosolar nitrogen. Astrophys. J. 553, L77–L79.

Owen, T., Mahaffy, P., Niemann, H.B., Atreya, S., Donahue, T., Bar-Nun, A., de Pater, I., 1999. A low-temperature origin for the planetesimals that formed Jupiter. Nature 402, 269–270.

Pollack, J.B., Hubickyj, O., Bodenheimer, P., Lissauer, J.J., Podolak, M., Greenzweig, Y., 1996. Formation of the giant planets by concurrent accretion of solids and gas. Icarus 124, 62–85.

Ragent, B., Colburn, D.S., Rages, K.A., Knight, T.C.D., Avrin, P., Orton, G.S., Yanamandra-Fisher, P.A., Grams, G.W., 1998. The clouds of Jupiter: results of the Galileo Jupiter mission probe nephelometer experiment. J. Geophys. Res. 103, 22891–22910.

Read, P.L., Conrath, B.J., Fletcher, L.N., Gierasch, P.J., Simon-Miller, A.A., Zuchowski, L. C., 2009. Mapping potential vorticity dynamics on Saturn: zonal mean circulation from Cassini and Voyager data. Planet. Space Sci. 57, 1682–1698.

Reuter, D.C., et al., 2007. Jupiter cloud composition, stratification, convection, and wave motion: a view from New Horizons. Science 318, 223.

Rinnert, K., Lanzerotti, L.J., Uman, M.A., Dehmel, G., Gliem, F.O., Krider, E.P., Bach, J., 1998. Measurements of radio frequency signals from lightning in Jupiter's atmosphere. J. Geophys. Res. 103, 22979–22992.

Roos-Serote, M., Vasavada, A.R., Kamp, L., Drossart, P., Irwin, P., Nixon, C., Carlson, R. W., 2000. Proximate humid and dry regions in Jupiter's atmosphere indicate complex local meteorology. Nature 405, 158–160.

Rousselot, P., et al., 2014. Toward a unique nitrogen isotopic ratio in cometary ices. Astrophys. J. 780, L17.

Sánchez-Lavega, A., et al., 2008. Depth of a strong jovian jet from a planetary-scale disturbance driven by storms. Nature 451, 437–440.

Sanchez-Lavega, A., Colas, F., Lecacheux, J., Laques, P., Parker, D., Miyazaki, I., 1991. The Great White SPOT and disturbances in Saturn's equatorial atmosphere during 1990. Nature 353, 397–401.

Saumon, D., Guillot, T., 2004. Shock compression of deuterium and the interiors of Jupiter and Saturn. Astrophys. J. 609, 1170–1180.

Scherer, S., Altwegg, K., Balsiger, H., Fischer, J., Jäckel, A., Korth, A., Mildner, M., Piazza, D., Reme, H., Wurz, P., 2006. A novel principle for an ion mirror design in time-of-flight mass spectrometry. International Journal of Mass Spectrometry 251, 73–81.

Seiff, A., Kirk, D.B., Knight, T.C.D., Young, R.E., Mihalov, J.D., Young, L.A., Milos, F.S., Schubert, G., Blanchard, R.C., Atkinson, D., 1998. Thermal structure of Jupiter's atmosphere near the edge of a 5−μm hot spot in the north equatorial belt. J. Geophys. Res. 103, 22857–22890.

Sentman, D.D., 1990. Electrical conductivity of Jupiter's shallow interior and the formation of a resonant of a resonant planetary-ionospheric cavity. Icarus 88, 73–86.

Showman, A.P., Dowling, T.E., 2000. Nonlinear simulations of Jupiter's 5-micron hot spots. Science 289, 1737–1740.

Simões, F., et al., 2012. Using Schumann resonance measurements for constraining the water abundance on the giant planets—implications for the solar system's formation. Astrophys. J. 750, 85.

Simon-Miller, A.A., Conrath, B., Gierasch, P.J., Beebe, R.F., 2000. A Detection of water ice on Jupiter with voyager IRIS. Icarus 145, 454–461.

Stevenson, D.J., Lunine, J.I., 1988. Rapid formation of Jupiter by diffuse redistribution of water vapor in the solar nebula. Icarus 75, 146–155.

Stevenson, D.J., Salpeter, E.E., 1977a. The dynamics and helium distribution in hydrogen–helium fluid planets. Astrophys. J. Suppl. Ser. 35, 239–261.

Stevenson, D.J., Salpeter, E.E., 1977b. The phase diagram and transport properties for hydrogen–helium fluid planets. Astrophys. J. Suppl. Ser. 35, 221–237.

Sromovsky, L.A., Baines, K.H., Fry, P.M., 2013. Saturn's Great Storm of 2010–2011: evidence for ammonia and water ices from analysis of VIMS spectra. Icarus 226, 402–418.

Sromovsky, L.A., Fry, P.M., 2010. The source of widespread 3−μm absorption in Jupiter's clouds: constraints from 2000 Cassini VIMS observations. Icarus 210, 230–257.

Sromovsky, L.A., Collard, A.D., Fry, P.M., Orton, G.S., Lemmon, M.T., Tomasko, M.G., Freedman, R.S., 1998. Galileo probe measurements of thermal and solar radiation fluxes in the jovian atmosphere. J. Geophys. Res. 103, 2929.

Sromovsky, L.A., Best, F.A., Revercomb, H.E., Hayden, J., 1992. Galileo Net Flux Radiometer experiment. Space Sci. Rev. 60 (1–4), 233–262.

Teanby, N.A., Fletcher, L.N., Irwin, P.G.J., Fouchet, T., Orton, G.S., 2006. New upper limits for hydrogen halides on Saturn derived from Cassini-CIRS data. Icarus 185, 466–475.

Tomasko, M.G., et al., 2002. The descent imager/spectral radiometer (DISR) experiment on the Huygens entry probe of titan. Space Sci. Rev. 104, 469–551.

Toyoda, M., Okumura, D., Ishihara, M., Katakuse, I., 2003. Multi-turn time-of-flight mass spectrometers with electrostatic sectors. J. Mass Spectrom. 38, 1125–1142.

Twarowski, A., 1995. Reduction of a phosphorus oxide and acid reaction set. Combust. Flame 102, 41–54.

Venot, O., Hébrard, E., Agúndez, M., Dobrijevic, M., Selsis, F., Hersant, F., Iro, N., Bounaceur, R., 2012. A chemical model for the atmosphere of hot Jupiters. Astron. Astrophys. 546, A43.

Visscher, C., Moses, J.I., Saslow, S.A., 2010. The deep water abundance on Jupiter: new constraints from thermochemical kinetics and diffusion modeling. Icarus 209, 602–615.

Visscher, C., Fegley Jr., B., 2005. Chemical constraints on the water and total oxygen abundances in the deep atmosphere of Saturn. Astrophys. J. 623, 1221–1227.

von Zahn, U., Hunten, D.M., Lehmacher, G., 1998. Helium in Jupiter's atmosphere: results from the Galileo probe helium interferometer experiment. J. Geophys. Res. 103, 22815–22830.

von Zahn, U., Hunten, D.M., 1992. The Jupiter Helium Interferometer experiment on the Galileo entry probe. Space Sci. Rev. 60 (1–4), 263–281.

Waite Jr., H., et al., 2014. A neutral gas investigation of origins (ANGIO), NASA AO NNH12ZDA006O-JUICE, Jupiter Icy Moons Explorer Instrument, submitted for publication.

Ward, W.R., 1997. Protoplanet migration by nebula tides. Icarus 126, 261–281.

Watkins, C., Cho, J.Y.-K., 2013. The vertical structure of Jupiter's equatorial zonal wind above the cloud deck, derived using mesoscale gravity waves. Geophys. Res. Lett. 40, 472–476.

Webster, C.R., et al., 2013. Isotope ratios of H, C, and O in CO_2 and H_2O of the Martian atmosphere. Science 341, 260–263.

Webster, C.R., Mahaffy, P.R., 2011. Determining the local abundance of Martian methane and its $^{13}C/^{12}C$ and D/H isotopic ratios for comparison with related gas and soil analysis on the 2011 Mars Science Laboratory (MSL) mission. Planet. Space Sci. 59, 271–283.

Weidenschilling, S.J., Lewis, J.S., 1973. Atmospheric and cloud structures of the Jovian planets. Icarus 20, 465–476.

West, R.A., Baines, K.H., Karkoschka, E., Sánchez-Lavega, A., 2009. Clouds and aerosols in Saturn's atmosphere. In: Saturn from Cassini–Huygens, p. 161.

West, R.A., Baines, K.H., Friedson, A.J., Banfield, D., Ragent, B., Taylor, F.W., 2004. Jovian clouds and haze. In: Jupiter. The Planet, Satellites and Magnetosphere, pp. 79–104.

Wilson, H.F., Militzer, B., 2012. Rocky core solubility in Jupiter and giant exoplanets. Phys. Rev. Lett. 108, 111101.

Wilson, H., Militzer, B., 2011. Solubility and erosion of icy cores in giant planets. In: APS Meeting Abstracts 31010.

Wilson, H.F., Militzer, B., 2010. Sequestration of noble gases in giant planet interiors. Phys. Rev. Lett. 104, 121101.

Wong, M.H., 2009. Comment on "Transport of nonmethane hydrocarbons to Jupiter's troposphere by descent of smog particles" by Donald M. Hunten [Icarus 194 (2008) 616 622]. Icarus 199, 231–235.

Wong, M.H., Mahaffy, P.R., Atreya, S.K., Niemann, H.B., Owen, T.C., 2004. Updated Galileo probe mass spectrometer measurements of carbon, oxygen, nitrogen, and sulfur on Jupiter. Icarus 171, 153–170.

Wright, I.P., et al., 2007. Ptolemy an instrument to measure stable isotopic ratios of key volatiles on a cometary nucleus. Space Sci. Rev. 128, 363–381.

Yair, Y., Fischer, G., Simões, F., Renno, N., Zarka, P., 2008. Updated review of planetary atmospheric electricity. Space Sci. Rev. 137, 29–49.

Yelle, R.V., Miller, S., 2004. Jupiter's thermosphere and ionosphere. In: Jupiter. The Planet, Satellites and Magnetosphere, pp. 185–218.

Zarnecki, J.C., Ferri, F., Hathi, B., Leese, M.R., Ball, A.J., Colombatti, G., Fulchignoni, M., 2004. In-flight performance of the HASI servo accelerometer and implications for results at Titan. In Proceedings of the International Workshop Planetary Probe Atmospheric Entry and Descent Trajectory Analysis and Science, ESA SP-544, 2004, pp. 71–76.